The Propagation and Evolution of Cyclonic Gulf Stream Rings

RICHARD P. MIED

Ocean Sciences Division, Naval Research Laboratory, Washington, DC 20375

GLORIA J. LINDEMANN

Research Computation Center, Naval Research Laboratory, Washington, DC 20375

(Manuscript received 2 May 1978, in final form 4 June 1979)

ABSTRACT

Numerical simulations of the propagation of cyclonic Gulf Stream rings are made using a primitive equation β-plane model of a flat-bottomed two-layer ocean with a rigid lid. Initially circular eddies having upper and deep ocean maximum currents $\max U_1$ and $\max U_2$ located at radial position l from the center are allowed to evolve and four types of behavior have been discerned: 1) dispersing rings possess negligible nonlinearity and disperse rapidly; 2) barotropic rings ($U_1 = U_2$) are weakly dispersive, propagating recognizably for long periods of time, and, nearly barotropic eddies ($U_1 \approx U_2$) slowly lose coherence in the deep ocean; 3) upper ocean rings propagate with a vortex present only in the upper ocean; and 4) eastward-traveling eddies possess circulations in the upper and lower oceans which propagate together stably to the east.

Changes in viscosity are found to be more important to the longevity of the ring than are changes in $(\max U_1)/\beta l^2$. Both westward and northward speeds increase with increasing $\max U_2/\max U_1$ and increasing $(\max U_1)/\beta l^2$. Speeds to the west are found to be 2–3 km day^{-1} and those to the north are 1–9 km day^{-1} for $3 \leq (\max U_1)/\beta l^2 \leq 15$ and $0 \leq \max U_2/\max U_1 \leq 1.2$.

1. Introduction

Cyclonic Gulf Stream rings are formed by a meander of the Gulf Stream into the Sargasso Sea which traps slope water in a closed ring of Stream water. Present evidence suggests that these cold core rings are probably formed at the rate of 5–8 per year (Fuglister, 1972) and that between 10 and 16 rings may be present at any one time (Lai and Richardson, 1977); they may thus cover about one-third of the northwestern Sargasso Sea. Their numbers and current speeds (of order 100 cm s^{-1}) suggest that a knowledge of the behavior of these rings may be very important to understanding the energetics of the western Atlantic Ocean in the vicinity of the Gulf Stream.

A modeling effort in this direction is that of Firing and Beardsley (1976) who have performed a numerical simulation of a barotropic cyclonic vortex on a beta-plane. Their work, which is corroborated with a linear calculation and a laboratory experiment, indicates that the eddy propagates in a northwesterly direction and generates an anticyclonic eddy behind it as it moves. A similar result is obtained by Bretherton and Karweit (1975) using a six-layer quasi-geostrophic model. A vortex in which the motion is cyclonic in the four uppermost layers and at rest in the lowest two is initialized over simulated MODE topography and observed to propagate northwest, while an anticyclonic motion evolves behind it. Few details of the propagation are given, although they do note that the eddy flow does not extend to the bottom. The role of the bottom topography in this process is not clear, however, and we shall discuss vertical coherence (or the lack of it) in Section 3.

In the present work, we attempt to numerically simulate the propagation and evolution of cyclonic Gulf String rings. The model assumes a two-layer, depth-averaged, primitive equation formulation on a beta plane. For initial conditions, we assume an interface displacement with Gaussian radial dependence and with geostrophically compatible upper and lower ocean velocities. The depths of the two layers, the deformation radius and the size of the eddy are fixed and chosen as fundamentally representative of those quantities found in the environment, while the eddy viscosity and relative layer velocities are varied among the experiments. The philosophy is thus that of thoroughly examining the behavior of the same typically sized eddy when a variety of velocity configurations are used as initial conditions. We find that the observed behaviors can differ significantly, one case from another.

Four fundamentally different propagation cases have been discerned; they are as follows:

a. Dispersing eddies

For very small fluid velocities an initially circular vortex may be viewed as a superposition of many Rossby waves and disperses as such (Firing and Beardsley, 1976; Flierl, 1977).

b. Barotropic and nearly barotropic eddies

Barotropic eddies possess equal velocities in the upper and the deep ocean, but disperse much less rapidly than linear eddies (type A above), propagating as recognizable entities for long periods of time. However, they do decay more rapidly than rings which contain both a baroclinic and a barotropic part. Nearly barotropic eddies are initialized with upper and lower ocean velocities which are directed in the same sense and with magnitudes close to one another. For the ratio of layer heights used in this paper they too disperse slowly, with the deep ocean flow decaying somewhat more rapidly than that of the upper ocean. Although the final state is presumed to be an upper ocean eddy of the type discussed in C below, the length of the experiments was necessarily too short to incontrovertibly establish this. Although this appears to be at odds with the concept of the barotropic cascade (Rhines, 1976), the fundamental reason for this difference will be discussed in Section 3.

c. Upper ocean eddies

If the velocities in the upper and lower ocean are significantly different, but still similarly directed initially, then the eddy structure in the deep ocean disperses rapidly and does not appear to reform for the duration of the experiment. The upper ocean flow, on the other hand, retains its vortex structure and concomitant interface displacement which propagate together as a stable entity in spite of the lack of a coherent structure in the deep ocean below (Mied, 1978a,b).

d. Eastward propagating eddies

A pure baroclinic circular vortex can evolve to an interesting mixed barotropic/baroclinic structure which propagates toward the east (Flierl, personal communication, 1978). Guided by this suggestion, the present authors attempted one such simulation, and also found that an initially baroclinic vortex exhibited a qualitatively similar behavior.

While an earlier draft (Mied, 1978a) of the current work was being revised for publication, the authors learned of a similar work nearing completion elsewhere (McWilliams and Flierl, 1979). That work seeks to model nonlinear vortices in general and their model employs the quasi-geostrophic equations in a two-layer ocean; their results may be more general than those of the present work in the sense that some parameters considered fixed in this paper (e.g., the ratio of the eddy length scale to the baroclinic deformation radius are allowed to vary in their research). The goal of their work is the exposition of the physics underlying the evolution of nonlinear vortices. In particular, they are concerned with the propagation and evolution of single- and mixed-mode vortices, and the evolution of an initially pure baroclinic vortex into an eastward-propagating structure.

The emphasis of the present work, on the other hand, is to employ a primitive equation model to examine the phenomenon of strong eddies (Gulf Stream rings in particular) and discussion is centered, for the most part, on the behavior of the upper ocean and deep ocean pressures and the interface displacement, which are related to those oceanic quantities (ocean velocities and isotherm displacement) most easily observed by researchers in the field. Because our motivation is the understanding of the propagation and evolution of Gulf Stream rings, the vortices examined have a variety of upper ocean and deep ocean velocities, but they are all cyclonically directed (with the exception of the single pure baroclinic case studied).

2. Preliminary considerations

The depth-averaged Boussinesq equations governing the motion of a two-layer ocean (without external forcing) may be written in the flux form (Grammeltvedt, 1969, O'Brien and Hurlburt, 1972)

$$\frac{\partial h_1 u_1}{\partial t} + \frac{\partial h_1 u_1 u_1}{\partial x} + \frac{\partial h_1 u_1 v_1}{\partial y} - h_1 f v_1 = -h_1 \frac{\partial P_1}{\partial x} + h_1 A_H \nabla^2 u_1, \tag{1a}$$

$$\frac{\partial h_1 v_1}{\partial t} + \frac{\partial h_1 v_1 u_1}{\partial x} + \frac{\partial h_1 v_1 v_1}{\partial y} + h_1 f u_1 = -h_1 \frac{\partial P_1}{\partial y} + h_1 A_H \nabla^2 v_1, \tag{1b}$$

$$\frac{\partial h_2 u_2}{\partial t} + \frac{\partial h_2 u_2 u_2}{\partial x} + \frac{\partial h_2 u_2 v_2}{\partial y} - h_2 f v_2 = -h_2 \frac{\partial P_1}{\partial x} + g' h_2 \frac{\partial h_1}{\partial x} + h_2 A_H \nabla^2 u_2, \tag{1c}$$

$$\frac{\partial h_2 v_2}{\partial t} + \frac{\partial h_2 v_2 u_2}{\partial x} + \frac{\partial h_2 v_2 v_2}{\partial y} + h_2 f u_2 = -h_2 \frac{\partial P_1}{\partial y} + g' h_2 \frac{\partial h_1}{\partial y} + h_2 A_H \nabla^2 v_2, \tag{1d}$$

$$\frac{\partial h_1}{\partial t} + \frac{\partial h_1 u_1}{\partial x} + \frac{\partial h_1 v_1}{\partial y} = 0, \tag{1e}$$

$$\frac{\partial h_2}{\partial t} + \frac{\partial h_2 u_2}{\partial x} + \frac{\partial h_2 v_2}{\partial y} = 0. \tag{1f}$$

The subscripts 1 and 2 refer to quantities in the upper and lower layers respectively; P_1 is the ratio of the upper layer pressure to a reference density [e.g., $\rho_0 = (\rho_1 + \rho_2)/2$]; A_H is the lateral coefficient of viscosity, which models subgrid-scale processes; f is the latitude-dependent Coriolis parameter; $g' = g(\rho_2 - \rho_1)/\rho_0$; and x and y are the zonal and meridional directions in which the velocities (u_i, v_i) are defined. A side view of this two-layer ocean with a flat bottom and rigid lid is given in Fig. 1. We see that the local layer thicknesses h_i are related to the interface displacement h and the undisturbed layer thicknesses H_i by

$$h_1 = H_1 - h, \quad h_2 = H_2 + h.$$

Finally, it is convenient to define a pressure P_2 in the deep ocean by

$$\nabla P_2 = \nabla P_1 + g' \nabla h.$$

We solve these equations numerically as a mixed initial-boundary value problem. By prescribing $h(x,y,t)$, $P_1(x,y,t)$, $u_i(x,y,t)$ and $v_i(x,y,t)$ at an initial time and imposing a free-slip boundary condition at the side walls, we see that the problem is well-posed. The proximity of the walls limits the length of time for which the experiment is valid, and this is discussed in Appendix B. The finite-differencing scheme has been formulated by Lilly (1965) for a barotropic ocean, and extended to a two-layer system by Holland and Lin (1975). The physical parameters which we use in this model ocean are given by

$H_1 = 1000$ m $\quad g' = 2$ cm s^{-2}

$H_2 = 4000$ m $\quad f = 7.3 \times 10^{-5}$ s^{-1}

$$+ 2 \times 10^{-13} \text{ cm}^{-1} \text{ s}^{-1} \times (y - y_0) \text{ [cm]}.$$

$A_H = 2.5 \times 10^5$ cm^2 s^{-1} for most experiments, although other values of A_H are used for the eddy dissipation studies; the internal radius of deformation is

$$\frac{1}{f_0}\left(\frac{gH_1H_2}{H_1 + H_2}\right)^{1/2} = 55 \text{ km}.$$

The integration is carried out in a 1000 km square box, so that $0 \leq x, y \leq 1000$ km. A time step of 20 min and grid spacing of 20 km are found to give a stable numerical solution and to adequately resolve the details of the eddy.

The interface displacement h and velocity fields (u_i, v_i) are chosen to be in geostrophic balance initially on an f plane. Although a more correct initial condition would require geostrophic balance on a beta-plane, our feeling is that because rings have such longevity in the ocean, the tendency for a stable configuration to form is strong and would not be severely influenced by a slight imbalance in the initial conditions. We do expect a readjustment of the flow shortly after initialization, however, and this is observed in many experiments.

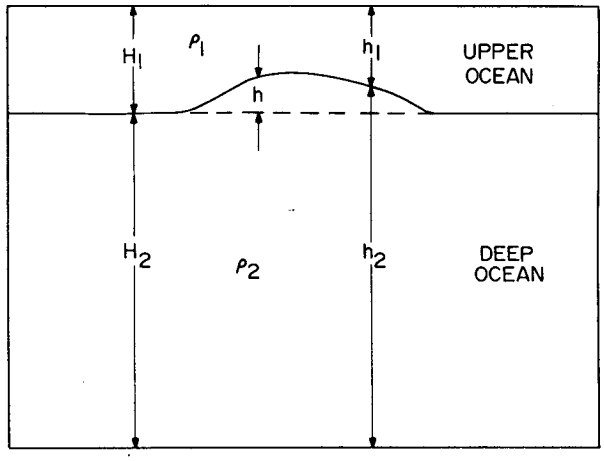

FIG. 1. A side view of the two-layer ocean showing the undisturbed layer heights H_1 and H_2 and interface displacement $h(x,y,t)$. The local upper and deep-ocean layer thicknesses are h_1 and h_2, while their densities are ρ_1 and ρ_2, respectively.

If we presume a plausible deep-ocean initial velocity field and interface displacement to be given by

$$\left.\begin{aligned} u_2 &= Ay \exp[-(x^2 + y^2)/2l^2] \\ v_2 &= -Ax \exp[-(x^2 + y^2)/2l^2] \\ h &= bH_1 \exp[-(x^2 + y^2)/2l^2] \end{aligned}\right\},$$

then we may calculate the pressure P_1 and the upper ocean velocity field (u_1, v_1) by imposing the above geostrophy argument. The values of A and b are then fixed by this argument. The upper ocean quantities are thus

$$\left.\begin{aligned} (u_1, v_1) &= (A + g'bH_1/f_0l^2)(y, -x) \\ &\quad \times \exp[-(x^2 + y^2)/2l^2] \\ P_1 &= (f_0Al^2 + g'bH_1) \exp[-(x^2 + y^2)/2l^2] \end{aligned}\right\}.$$

Note that for a cyclonic motion ($A < 0$) with $|u_1^2 + v_1^2| > |u_2^2 + v_2^2|$, $b < 0$. The maximum velocities in the top and bottom layers are respectively

$$(A + g'bH_1/f_0l^2)le^{-1/2} \quad \text{and} \quad Ale^{-1/2}$$

which occur at radius $= l$.

A fairly representative eddy diameter appears to be O(250 km). By requiring that 90% of the amplitude variation of the initial fields be contained within a radius of 125 km, we see that $(x^2 + y^2)^{1/2}/2^{1/2}l = 1.5$, so that $l = 250/3\sqrt{2}$ or 58.9 km. With the eddy size

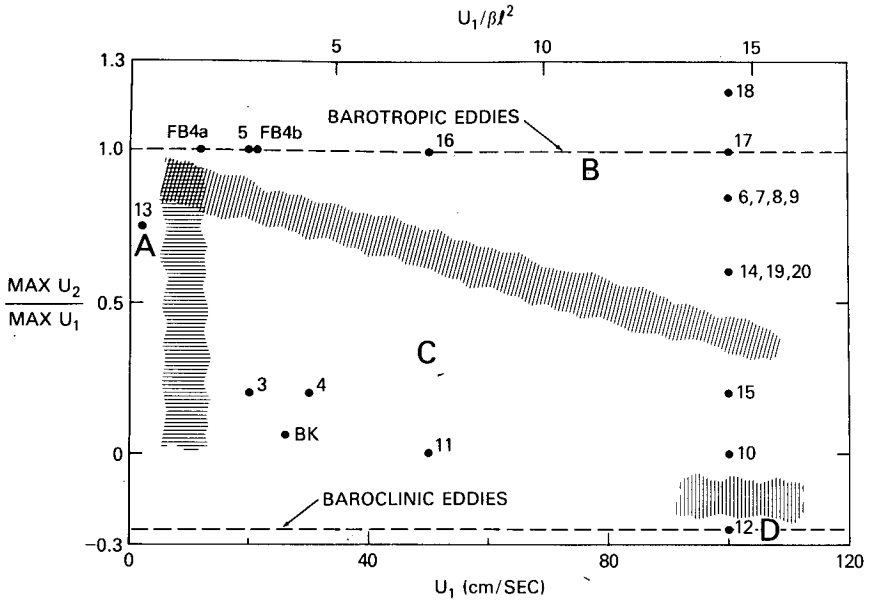

FIG. 2. Initial velocity ratio ($\max U_2/\max U_1$) vs. strength (U_1), also given as $U_1/\beta l^2$ with $\beta = 2 \times 10^{-13}$ cm^{-1} s^{-1} and $l = 58.9$ km. The numbers beside each dot indicate the experiment number. The dashed lines corresponding to an initially pure barotropic and baroclinic motion are shown, as are the experiments of Firing and Beardsley (1976) and Bretherton and Karweit (1975). (See Appendix A.) The lettered areas indicate four different types of vortex behavior: A, dispersing eddies; B, barotropic or nearly barotropic eddies; C, upper ocean eddies; D, eastward propagating eddies.

now fixed, there remain only two free parameters (apart from the eddy viscosity A_H); these are (max $\times$ U_2)/(maxU_1)[1], a measure of the relative barotropy, and $U_1/\beta l^2$, a measure of the nonlinearity, or relative magnitude of the advective terms and the variation of the Coriolis parameter with latitude. Using these two quantities, we can display a plane which gives an overview of the experiments (Fig. 2). The experiments of Bretherton and Karweit (1975) and Firing and Beardsley (1976) (see Appendix A) are shown in relation to the present work. The shading is meant to generally delineate one region of the parameter space from another, in which the actual boundaries are only poorly known. A complete list of the experiments, showing current speeds in each layer is given in Table 1.

3. The regimes of propagation and evolution

As mentioned in Section 2, an isolated interface displacement anomaly with Gaussian radial dependence and geostrophically compatible currents in the upper and lower oceans is situated in the 1000 km square box and allowed to evolve. As we shall see below, the resulting motions can exhibit very different characteristics depending upon the initial conditions, and some of these flow configurations are quite startling. In particular, four basic classes of motion have been observed thus far; and these could be identified as dispersing eddies, barotropic or nearly barotropic eddies (which presumably evolve to upper ocean eddies), upper ocean eddies, and an eastward-propagating eddy. A description of an experiment on each type is listed below.

a. Dispersing eddies

The analytical calculations of Flierl (1977) and Firing and Beardsley (1976) clearly show that when vortices are governed by linear dynamics, they disperse, their energy being radiated away from the initial eddy by the constituent Rossby waves. It follows that the present nonlinear model would exhibit similar behavior if the current magnitudes were small, so that the ratio of nonlinear to linear terms would be insignificant. This is observed to be the case. In experiment 13, the upper and lower depth-averaged velocities are 2.0 and 1.5 cm s^{-1}. The results of this experiment (hereafter referred to as EXP 13, or a 2/1.5 eddy) are shown in Fig. 3 for the first 50 days. There is little difference between the sequence for the upper pressure (proportional to the streamfunction for small Rossby numbers) shown in Fig. 3a and the lower pressure field in Fig. 3b. The dispersion is qualitatively similar to that ob-

[1] $U_i = (u_i^2 + v_i^2)^{1/2}$. $U_1/\beta l^2$ is to be taken as a succinct form of $(\max U_1)/\beta l^2$.

TABLE 1. Synopsis of the experiments and approximate relation of work of Bretherton and Karweit (1975) and Firing and Beardsley (1976) to present paper (see Appendix A). Cyclonic currents are positive, anticyclonic negative. Blanks for parameter values indicate no change from previous case.

Experiment	U_1 (cm s^{-1})	U_2 (cm s^{-1})	$U_1/\beta l^2$	A_H (cm^2 s^{-1})	Comments
3	20	4	2.88	2.5×10^5	Upper ocean eddy
4	30	6	4.32		Upper ocean eddy
5	20	20	2.88		Pure barotropic
6	100	85	14.41		Evolves to upper ocean eddy (?)
7					Tests influence of wall proximity
8					Tests influence of wall proximity
9					Tests influence of wall proximity
10		0			Upper ocean eddy
11	50		7.21		Upper ocean eddy
12	100	−25	14.41		Propagates eastward (after McWilliams and Flierl, 1979)
13	2	1.5	0.29		Dispersing eddy
14	100	60	14.41		Evolves to upper ocean eddy (?)
15	100	20			Upper ocean eddy
16	50	50	7.21		Pure barotropic
17	100	100	14.41		Pure barotropic
18		120			Evolves to upper ocean eddy (?)
19		60		5×10^5	Tests influence of viscosity
20				2.5×10^6	Tests influence of viscosity
BK	17.7	0.58	3.77	—	Bretherton and Karweit (1975)
FB4a	U_1	$=U_2$	1.70	—	Firing and Beardsley (1976) their Fig. 4a
FB4a	U_1	$=U_2$	3.03	—	Firing and Beardsley (1976) their Fig. 4b

served by Flierl (1977) and Firing and Beardsley (1976), and this is not surprising because $U_1/\beta l^2 = 0.29$, a small value in relation to that of the other experiments. There is thus evidently insufficient nonlinearity to render the eddy a coherent structure, and the radiated baroclinic and rapidly propagating barotropic waves show wall interference as early as day 10. We note that the eddy, which was not initially centered in the box, exhibits considerable asymmetry and wall influence by day 50. The important point, however, is that the energy in the eddy has dispersed instead of remaining fairly localized. This type of behavior occurs in the region of the parameter space labeled A (Fig. 2).

A more quantitative measure of the dispersive process can be made by comparing the time record of the extremum in the baroclinic pressure with that obtained from the linearized quasi-geostrophic calculation (Appendix A). A comparison between these two results is shown in Fig. 4 for 25 days. We note that the two curves agree rather well, with the result of EXP 13 falling below that of the theory. We attribute the somewhat more rapid roll-off of P_{BC} in EXP 13 to the viscosity A_H, which is quite large.

b. Barotropic and nearly barotropic eddies

There are a limited number of analytical simulations of the evolution of vortices on a beta plane which suggest that the eddy must be sufficiently nonlinear, i.e., $U_1/\beta l^2 \gg 1$, to persist and propagate as a recognizable entity. The stationary, barotropic modons[2] of Stern (1975), for example, arise from a balance between the advection of fluid particles up or down the planetary vorticity gradient ($\beta\psi_x$) and and advection of relative vorticity $[\partial(\psi,\nabla^2\psi)/\partial(x,y)]$. Larichev and Reznik (1976) and Firing and Beardsley (1976) similarly show that the motion must be considered as intrinsically nonlinear; otherwise, a propagating eddy cannot exist.

In our model, this is accomplished by increasing $\max U_1$, because β and l are given fixed representative values. A barotropic eddy is initiated by putting $\max U_1 = \max U_2$ and setting $g' = 0$. Such an experiment has been performed on a 20/20 eddy ($U_1/\beta l^2 = 2.88$) in EXP 5 and the contours of constant pressure are shown for the first 50 days in Fig. 5.

As the eddy begins to evolve and propagate, we see evidence of some of the dispersive features present in the linear case described above. The eddy becomes elongated on its western side and an anticyclonic feature is formed to the east of the original vortex. The westward propagation of these features is a consequence of β, while the rate of northward propagation of a cyclonic vortex is determined by the strength of the currents (Bretherton, 1975). In this experiment involving only moderate

[2] Stern uses modon to denote a pair of barotropic vortices with the counterclockwise vortex to the north of the clockwise one. Their strengths and shapes are adjusted so that their mutual advection toward the east exactly balances their westward β-tendency.

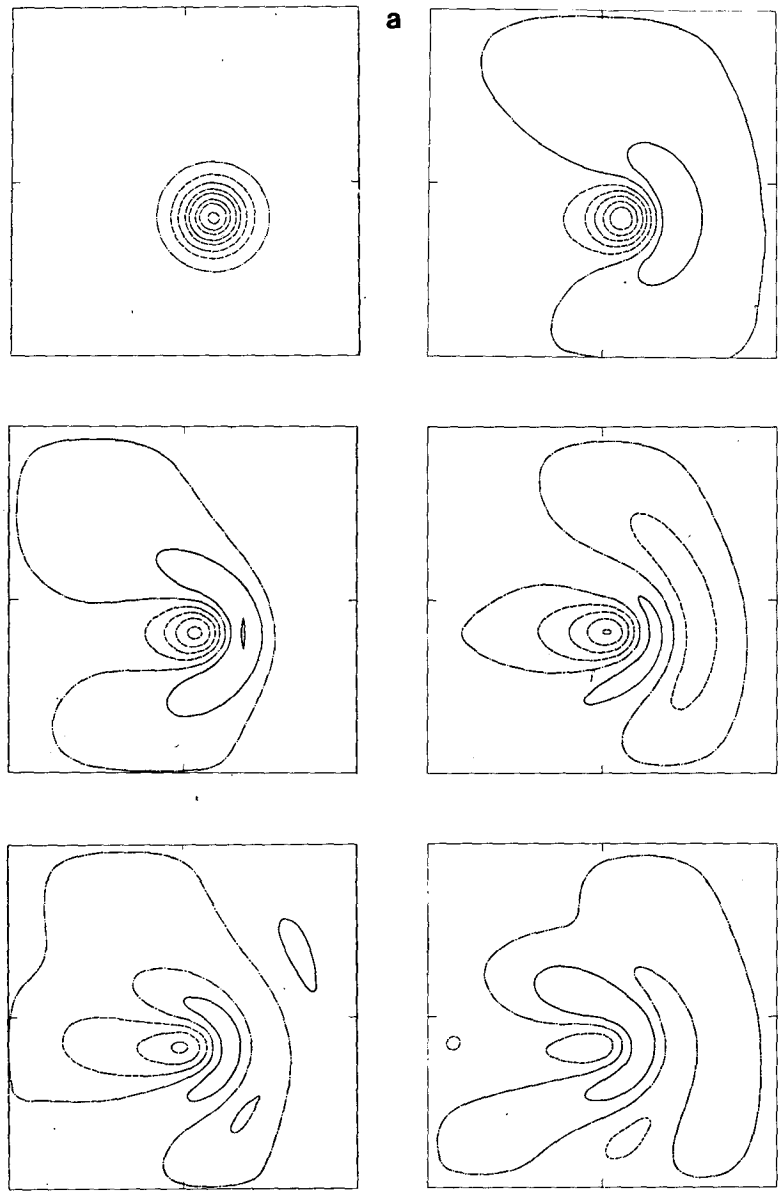

FIG. 3a. Contours of upper ocean pressure (P_1) for EXP 13 at day 0 and every 10 days thereafter. Contour level = 1.8×10^{-2} m^2 s^{-2}. Contour code (——) for $P_1 > 0$, (– – –) for $P_1 = 0$ and (-----) for $P_1 < 0$.

nonlinearity, the northward propagation is clearly evident. From Fig. 2, we see that EXP 5 is parametrically similar to Firing and Beardsley's (1976) Fig. 4b. For comparison, the streamlines of their experiment at 33.6 days (see Appendix A) are shown in our Fig. 6. The similarity of the streamlines in Fig. 6 and the constant-pressure contours of EXP 5 at day 30 (Fig. 5) is striking. Because all the radiated waves are rapidly traveling barotropic ones, we are not surprised that the influence of the wall on the waves dispersing from the initial configuration is evident in only 10 days. The significant point to be made, however, is that the larger value of $U_1/\beta l^2$ results in a coherently propagating eddy, which is readily identifiable after 50 days.

Closely related to these pure barotropic eddies are those in which $\max U_1$ and $\max U_2$ are sufficiently close at the outset so that the resulting slowly evolving structure bears a resemblance to pure barotropic eddies. The resemblance is only superficial, however, because an evolution to a barotropic state is not observed. Although the experiments are of insufficient duration to determine the ultimate fate of the eddy, we can see from EXP 7 (Fig. 7) that the

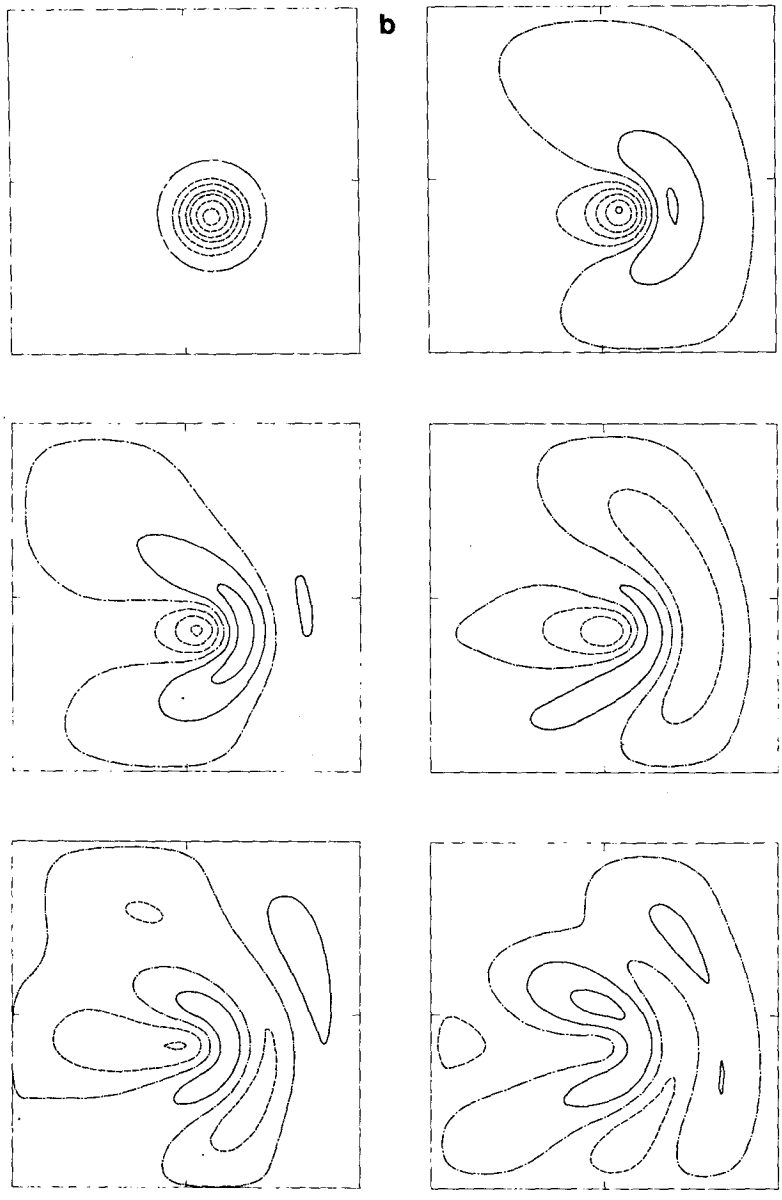

FIG. 3b. Contours of lower ocean pressure (P_2) for EXP 13 at day 0 and every 10 days thereafter. Contour level = 1.5×10^{-2} m^2 s^{-2}. See Fig. 3a for contour code.

central eddy pressure in the deep ocean decays more rapidly than that in the upper ocean. Our conjecture that an evolution to barotropy does not occur appears to disagree with trends observed by Rhines (1976). The mechanics of Rhines' barotropic cascade are most readily seen from the quasi-geostrophic equations (see Appendix A).

$$\frac{d}{dt}\nabla^2\psi_1 = -F_1\frac{d}{dt}(\psi_2 - \psi_1) - \beta\frac{\partial\psi_1}{\partial x},$$

$$\frac{d}{dt}\nabla^2\psi_2 = -F_2\frac{d}{dt}(\psi_1 - \psi_2) - \beta\frac{\partial\psi_2}{\partial x},$$

where

$$F_i = \frac{f_0^2}{g'H_i}.$$

To this approximation (Holland, 1978),

$$F_i\frac{d}{dt}(\psi_2 - \psi_1) = \frac{f_0}{H_i}\frac{dh}{dt}$$

so that

$$\frac{d\nabla^2\psi_1}{dt} = -\frac{f_0}{H_1}\frac{dh}{dt} - \beta\frac{\partial\psi_1}{\partial x},$$

$$\frac{d\nabla^2\psi_2}{dt} = +\frac{f_0}{H_2}\frac{dh}{dt} - \beta\frac{\partial\psi_2}{\partial x}.$$

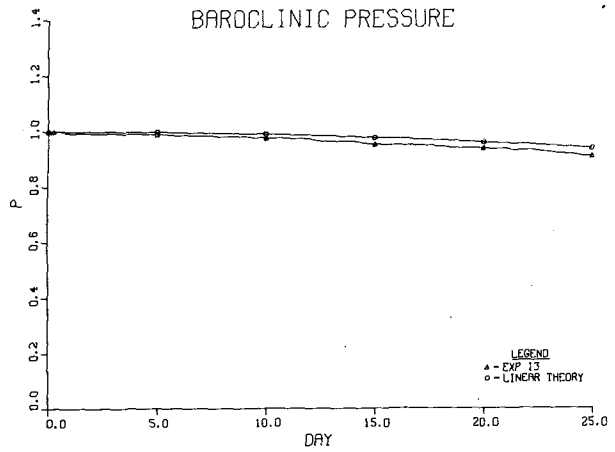

An upper ocean cyclonic vortex ($\nabla^2\psi_1 > 0$) is accompanied by an elevation in the thermocline ($h > 0$) provided $\psi_2 > \psi_1$. As it propagates northward and westward the vortex stretching effect of the upper ocean on the lower ocean at the forward edge of the eddy should act as a source of vorticity $[(f_0/H_2)(dh/dt) > 0]$ so that deep ocean fluid particles should begin to rotate cyclonically ($d/dt\nabla^2\psi_2 > 0$). One would thus expect that a tendency to establish barotropy would occur for the nearly barotropic eddies in region B of Fig. 2. This is not

FIG. 4. Comparison between the barotropic pressure (P_{BT}) (see Appendix A) for EXP 13 and the linearized quasi-geostrophic result for a dispersing eddy.

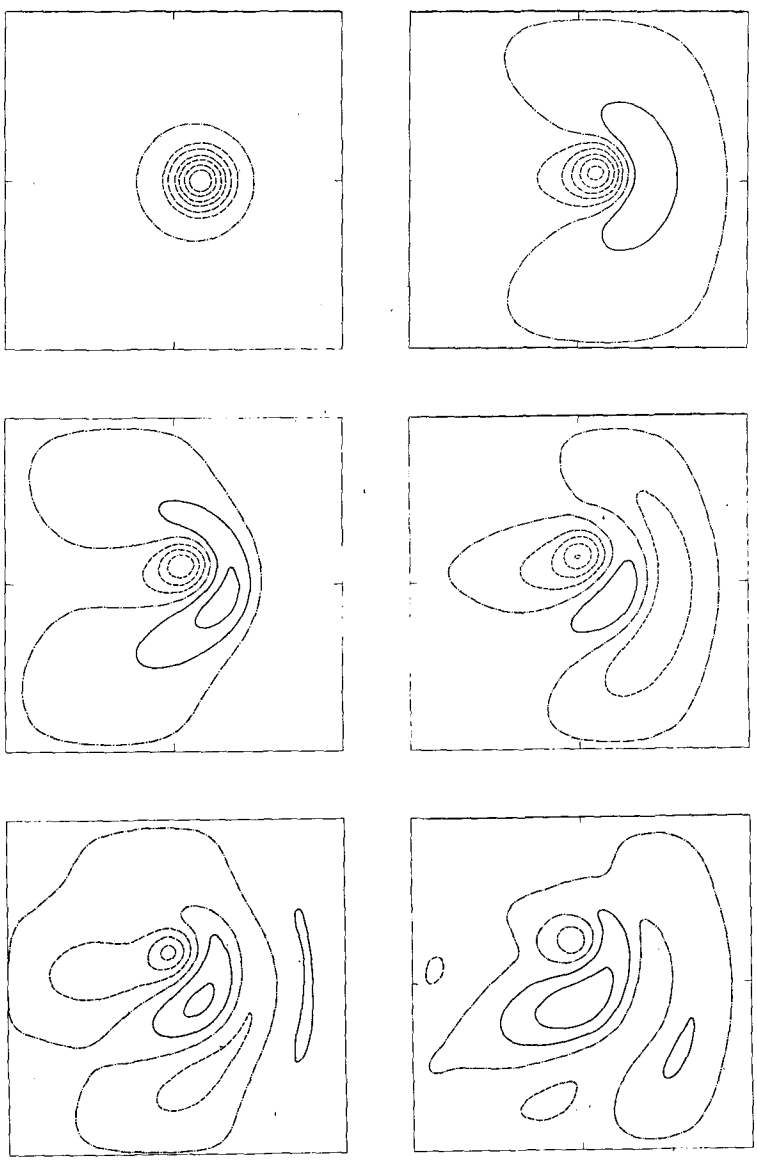

FIG. 5. Contours of constant pressure for the barotropic eddy (20/20) of EXP 5; contour level = 0.2 m^2 s^{-2}. The influence of the boundaries is felt as early as day 10, but the eddy is clearly discernable at day 50.

necessarily seen to be the case for an individual eddy, however. In fact, the pressure records for the eddies indicate that an experiment of greater duration would show that the deep ocean flow bears no resemblance to that of the upper ocean. This is evident in the very early time history of the eddies in region C and we shall discuss their behavior and the barrier to the expected barotropic cascade below.

c. *Upper ocean eddies*

It can happen that for some regions of the parameter space in Fig. 2, the upper ocean can sustain an eddying motion and related interface displacement which propagate stably, while no similar vortex is ever present for any length of time in the deep ocean. This tendency can be better understood by examining the quasi-geostrophic equations. When these are nondimensionalized in the manner indicated in Appendix A, they may be written

$$\frac{\partial}{\partial \hat{t}}\left[\nabla^2\hat{\psi}_1 + \frac{f_0^2 l^2}{g' H_1}(\hat{\psi}_2 - \hat{\psi}_1)\right] + \frac{\partial \hat{\psi}_1}{\partial \hat{x}} + \frac{U}{\beta l^2} J\left[\hat{\psi}_1, \nabla^2\psi_1 + \frac{f_0^2 l^2}{g' H_1}(\hat{\psi}_2 - \hat{\psi}_1)\right] = 0,$$

$$\frac{\partial}{\partial \hat{t}}\left[\nabla^2\hat{\psi}_2 + \frac{f_0^2 l^2}{g' H_2}(\hat{\psi}_1 - \hat{\psi}_2)\right] + \frac{\partial \hat{\psi}_2}{\partial \hat{x}} + \frac{U}{\beta l^2} J\left[\hat{\psi}_2, \nabla^2\hat{\psi}_2 + \frac{f_0^2 l^2}{g' H_2}(\hat{\psi}_1 - \hat{\psi}_2)\right] = 0.$$

In the limit $H_1/H_2 \ll 1$, the vortex stretching effect in the deep ocean can then be seen to be very much smaller than when $H_1 \approx H_2$. This shallow thermocline limit then provides a situation in which the lower ocean is decoupled from the upper ocean and thus behaves essentially like a barotropic fluid. If in addition, $U_2/\beta l^2$ is not large, then there may be insufficient nonlinearity to sustain this barotropic-like eddy in the deep ocean, and the lower part of the initial ring can disperse. In the absence of strong coupling between the layers, it will probably not reform. McWilliams and Flierl (1979) discuss this effect in a more quantitative fashion by appropriately scaling $\hat{\psi}_1$ and $\hat{\psi}_2$ and pursuing an asymptotic expansion of the equations in powers of $(H_1/H_2)^{1/2}$.

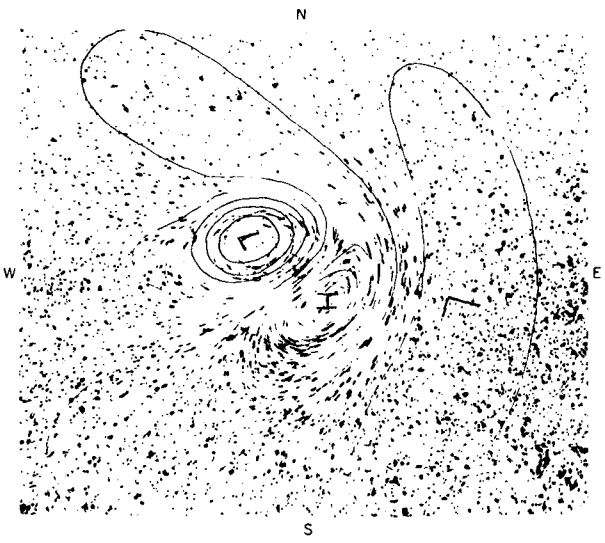

FIG. 6. The streamlines of Firing and Beardsley's (1976) experiment shown in their Fig. 4b. This picture is equivalent to an elapsed time of 33.6 days and $U_1/\beta l^2 = 3.03$ in the present work (see Appendix A).

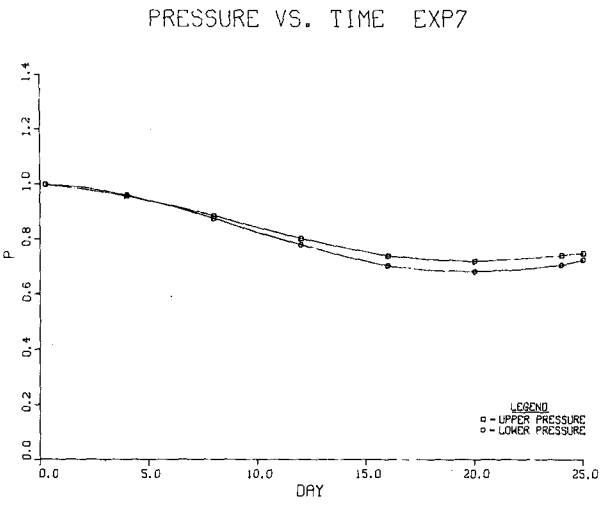

FIG. 7. The upper ocean pressure $P_1(t)$ and deep-ocean pressure $P_2(t)$ for EXP 7.

A particularly interesting experiment which illustrates this phenomenon is EXP 3 (a 20/4 ring). In Fig. 8, the interface displacement is shown for 150 days, and we can see that despite serious wall influence after 70 days, the eddy is quite persistent. A time series of the upper ocean pressure contours P_1 (Fig. 9) over the same time interval reveals a similar pattern which, as expected, is equally persistent. The deep ocean pressure field P_2 (Fig. 10), however, exhibits the very rapid barotropic-like dispersion of the initial ring configuration, with some of the radiating Rossby waves reaching the wall within the first 10 days. We note that during the entire five months of the experiment, no vortex was generated in the lower ocean which appeared connected with that in the upper ocean. The time histories of the central pressures P_1 and P_2 underscore this fact. In Fig. 11, we see the minimum $P_1(t)$ and $P_2(t)$ associated with the eddy for 150 days. Although the walls of the box severely contaminate the signals in the upper and deep ocean after about 25 days, the persistence of the slowly decaying upper ocean vortex is evident. In contrast to this, the deep ocean pressure directly beneath the upper ocean vortex falls off rapidly and then appears to fluctuate about a zero value.

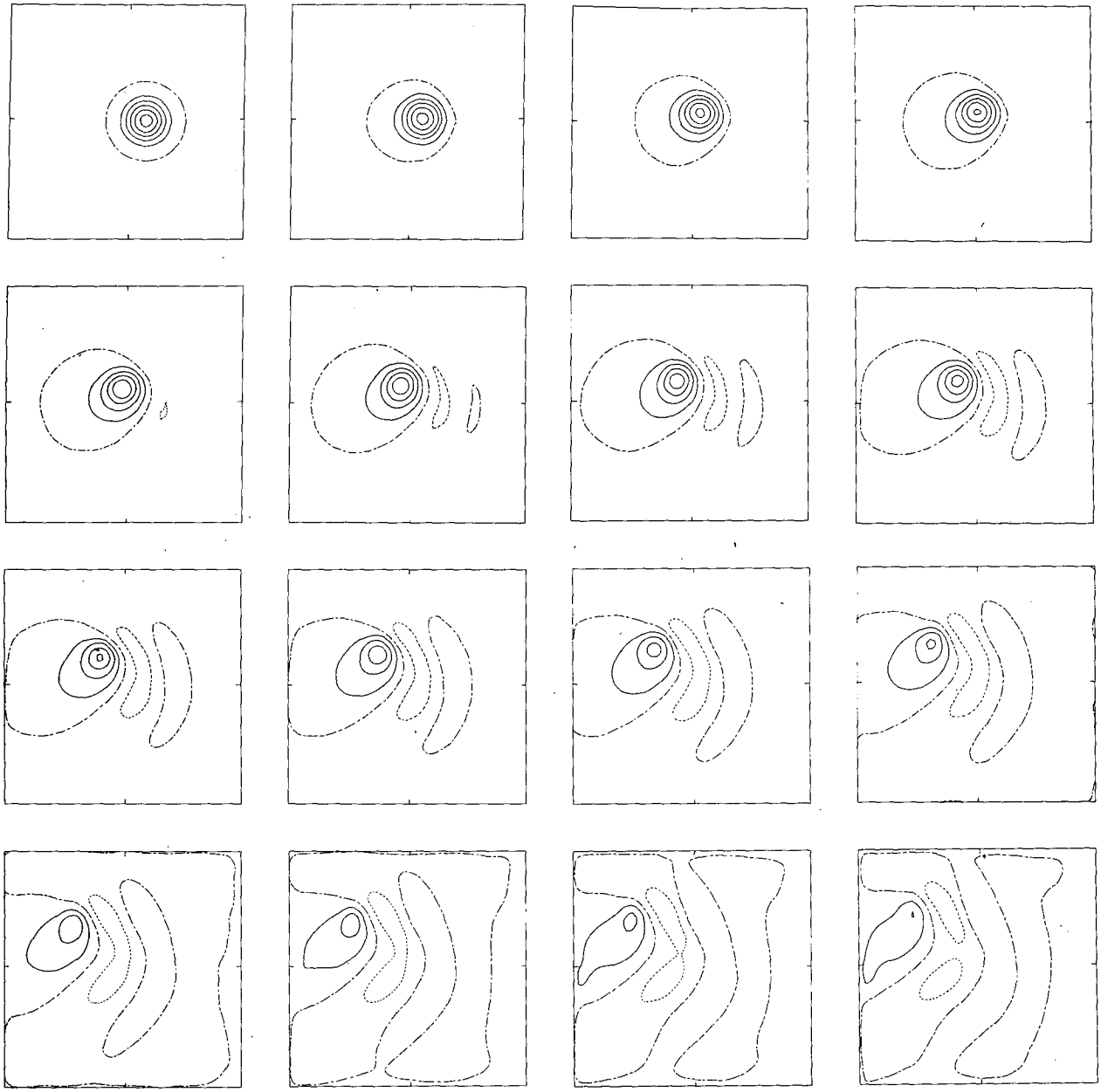

FIG. 8. Interface displacement evolution $h(x,y,t)$ in EXP 3 for 150 days, shown at $t = 0$ and every 10 days thereafter. Contour level = 10 m. Contour code (-----) for $h < 0$; (– - –) for $h = 0$ and (——) for $h > 0$.

Given the ineffective coupling between the two layers ($H_1/H_2 = 0.25$) and the small nonlinearity in the deep ocean ($U_2/\beta l^2 = 0.58$) the rapid disintegration of the deep-ocean counterpart of the upper ocean eddy and its inability to reestablish itself is not too surprising. The reader will note from Fig. 2 that EXP BK (Bretherton and Karweit, 1975) falls within this parameter range and should, in fact, be grouped with the upper ocean eddies. This would be consistent with their statement that "no persistent or remarkable structure appeared below the vortex in deep water," although the role of the bottom topography in their simulation is unclear.

d. Eastward propagating eddies

That an initially circular, pure baroclinic vortex can spin up an eastward-traveling structure consisting principally of a barotropic modon (Larichev and Reznik, 1976) with an accompanying baroclinic gyre has already been thoroughly documented by McWilliams and Flierl (1979).

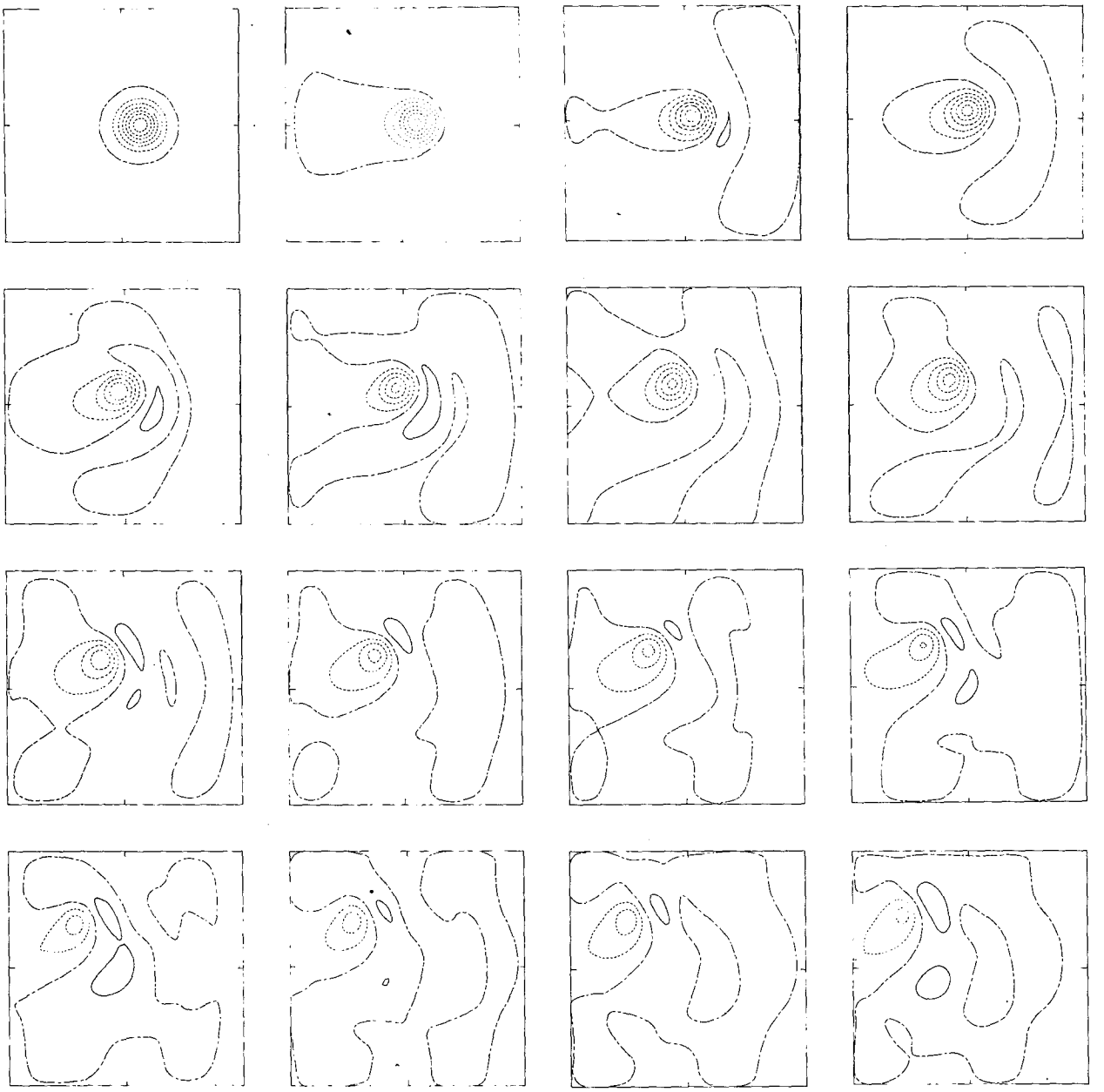

FIG. 9. Upper ocean pressure P_1 for EXP 3 at 10 day intervals for 150 days. Contour level = 0.2 m^2 s^{-2}. Contour code (-----) for $P_1 < 0$; (– - –) for $P_1 = 0$; and (——) for $P_2 > 0$.

We have subsequently attempted a simulation of this sort with our primitive equation model (EXP 12—a 100/(−25) eddy) and, indeed, the trajectories of the upper and deep ocean gyres (Fig. 12) indicate that propagation is toward the east, and very slightly northward. At day 150, the contours of constant upper ocean pressure (Fig. 13a) are nearly circular, while those for the deep ocean (Fig. 13b) are very much distorted; the initial sense of rotation of the gyres is preserved, however. The barotropic and baroclinic pressures (Figs. 13c and 13d) are at least qualitatively similar to the patterns discussed by McWilliams and Flierl.

Flierl *et al.* (1980) have shown that the quasi-geostrophic two-layer equations admit many types of solutions, among them the familiar barotropic modon[3] solution of Larichev and Reznik (1976) and a

[3] In this context, we are referring to the work of Larichev and Reznik who show that the two stationary vortices of Stern (his modon) can propagate steadily toward the east when the effect of their mutual advection is sufficiently strong to overcome the westward β-tendency.

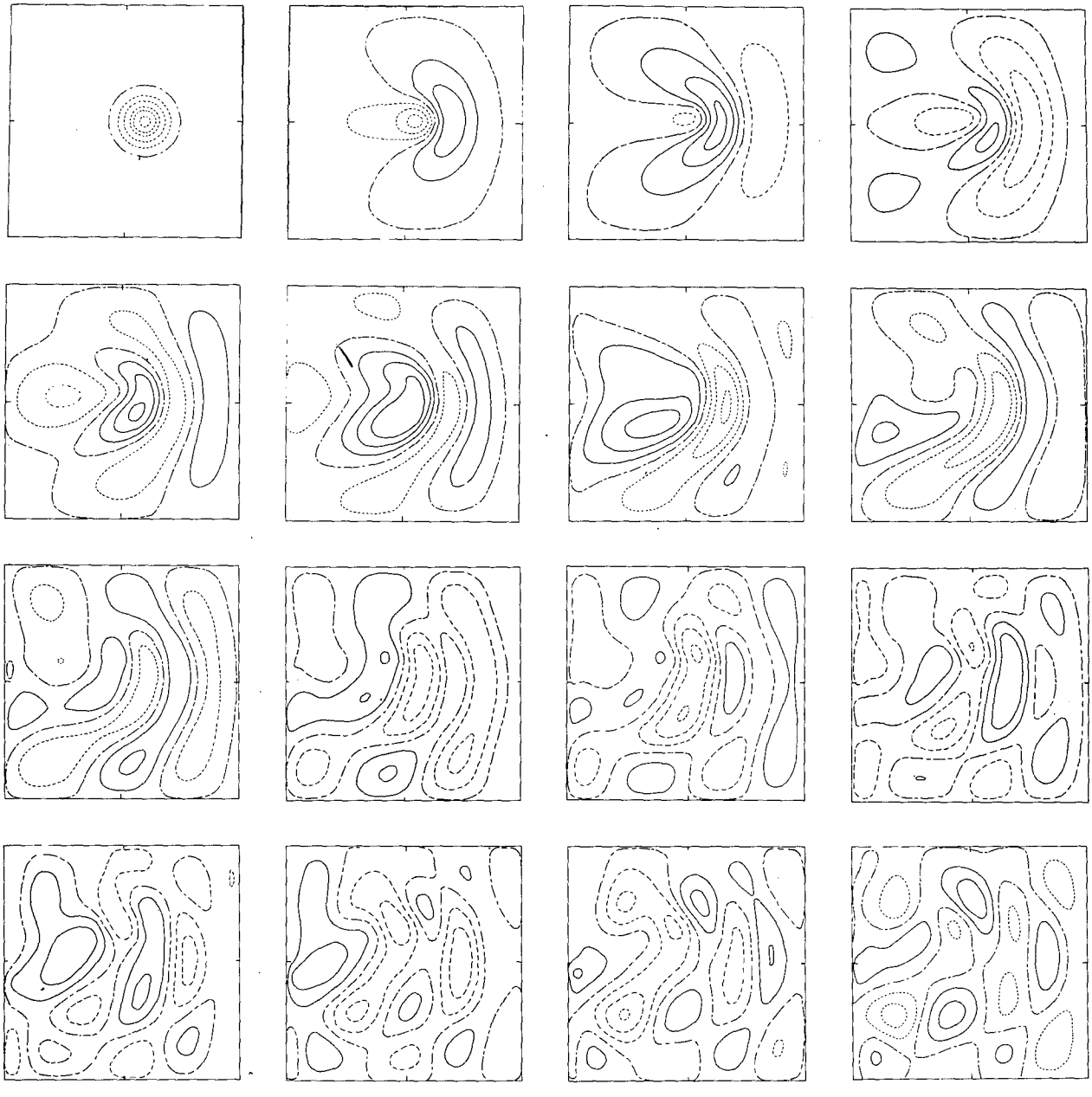

FIG. 10. The deep ocean pressure P_2 at 10 day intervals for 150 days. Contour level = 0.05 m^2 s^{-2}. Contour code (-----) for $P_2 < 0$; (– · –) for $P_2 = 0$; and (——) for $P_2 > 0$.

circular baroclinic vortex which they term a "rider." These solutions are obtained by requiring that the pressure and its radial derivative be continuous at the streamline dividing the interior and the exterior flow.

Examination of the quantities $\nabla^2 P_{BT}$ and $\nabla^2 P_{BC}$ for EXP 12 indicates that these quantities too are continuous, or at least appear to be so. To examine the influence of also imposing the restriction of the continuity of vorticity upon the dispersion relation of the barotropic/baroclinic modon of EXP 12, we examine the steady quasi-geostrophic equations (Appendix A) for the baroclinic and barotropic parts translating toward the east with speed U; their first integrals are

$$\nabla^2\psi_{BT} + \beta\eta = -\begin{pmatrix}\kappa^2\\ \rho^2\end{pmatrix}(\psi_{BT} + U\eta), \quad r \lesseqgtr a,$$

$$\nabla^2\psi_{BC} + \begin{pmatrix}\alpha^2\\ -\gamma^2\end{pmatrix}\psi_{BC} = \mu, \quad r \lesseqgtr a,$$

where $R_d = (F_1 + F_2)^{-1/2}$, $\alpha^2 = \kappa^2 - R_d^{-2}$, μ = constant and $\gamma^2 = -\rho^2 + R_d^{-2}$. The equivalence $-\rho^2 = \beta/U$

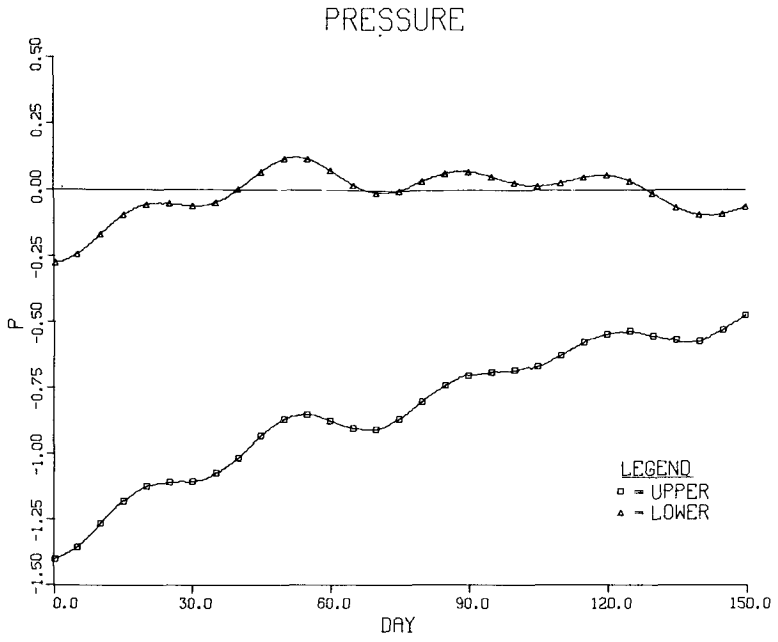

FIG. 11. P_1 and P_2 for EXP 3 (a 20/4 ring) shown in *dimensional* units ($m^2\ s^{-2}$) for 150 days.

arises from the barotropic work of Larichev and Reznik which is unchanged in the present context. The baroclinic solutions of Flierl *et al.* (1980) are (to within a constant)

$$\psi_{BC} = AJ_0(\alpha r) + \mu/\alpha^2, \quad r < a,$$

$$\psi_{BC} = BK_0(\gamma r) + \mu/r^2, \quad r > a,$$

which are the propagating, two-layer equivalent of the stationary solutions for continuous stratification first derived by Flierl (1976). The imposition of his constraints (that ψ_{BC} and $\partial\psi_{BC}/\partial r$ be continuous at $r = a$) can be combined with our additional restriction that $\nabla^2\psi_{BC}$ be continuous there also. We thus obtain a set of three linear, homogeneous equations for A, B, and μ whose determinant must vanish. This, along with familiar Bessel identities, yields the dispersion relation

$$\frac{J_1(\alpha a)}{(\alpha a)J_0(\alpha a)} + \frac{K_1(\gamma a)}{(\gamma a)K_0(\gamma a)} = 0,$$

which may be combined with the usual barotropic relation

$$\frac{J_2(a\kappa)}{(a\kappa)J_1(a\kappa)} + \frac{K_2(a\beta^{1/2}/U^{1/2})}{\left(\dfrac{a\beta^{1/2}}{U^{1/2}}\right)K_1(a\beta^{1/2}/U^{1/2})} = 0.$$

These two dispersion relations may be solved together to relate the speed $U/\beta R_d^2$ and the modon radius a/R_d.[4]

The modon has traveled about 68 km east in 50 days, so that for $\beta = 2 \times 10^{-13}$ cm and $R_d = 55$ km, $U/\beta R_d^2 = 0.260$. The radius a appears to be 162 km, so that $a/R_d = 2.945$. Given this value for the radius, reference to the table of roots indicates that the predicted value of $U/\beta R_d^2 = 0.32$, which corresponds to a propagation rate of 1.94 cm s^{-1} east. Compared with the observed figure of 1.57 cm s^{-1}, the lack of precise agreement seems reasonable

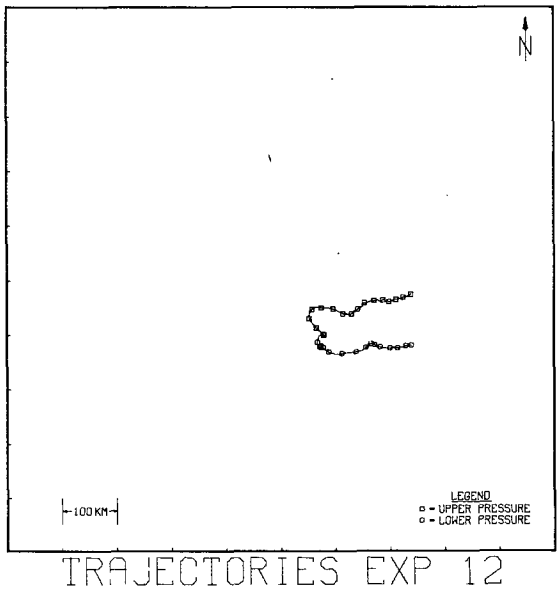

FIG. 12. Trajectories of P_1 and P_2 for 150 days for EXP 12. Data points occur at 10 day intervals.

[4] Prof. G. R. Flierl has done this and kindly provided us with a table of the roots.

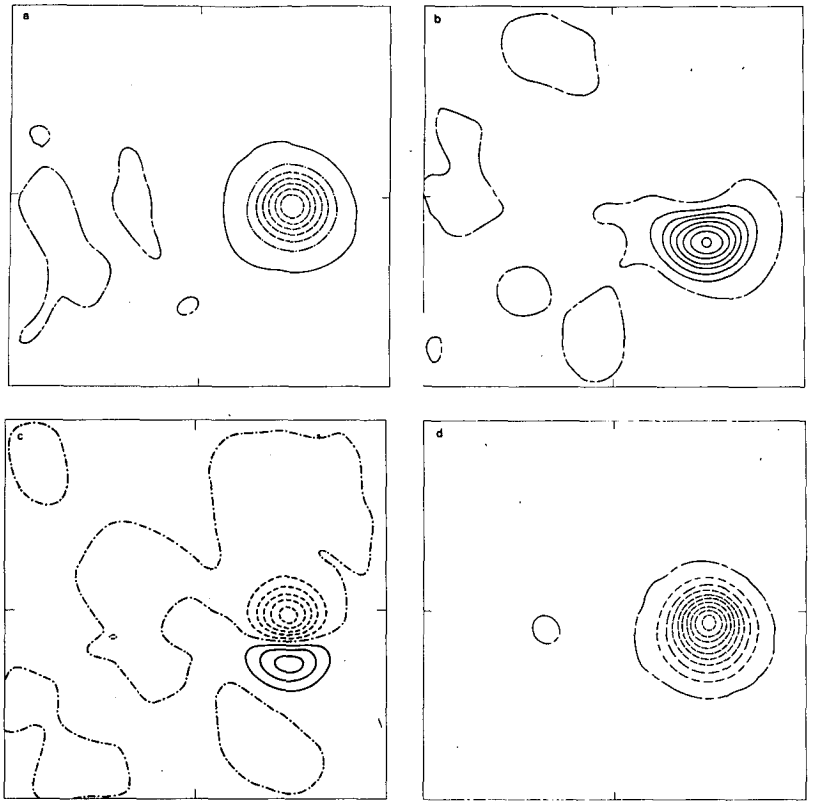

FIG. 13. Contours of constant pressures for EXP 12 at 150 days. (a) P_1 contour level = 1.0 m^2 s^{-2}. The only positive P_1 contour level = 0.25 m^2 s^{-2}. (b) P_2 contour level = 0.2 m^2 s^{-2}. (c) P_{BT} contour level = 0.25 m^2 s^{-2}. (d) P_{BC} contour level = 0.3 m^2 s^{-2}. Contour codes (-----) for $P < 0$; (– – –) for $P = 0$, and (——) for $P > 0$.

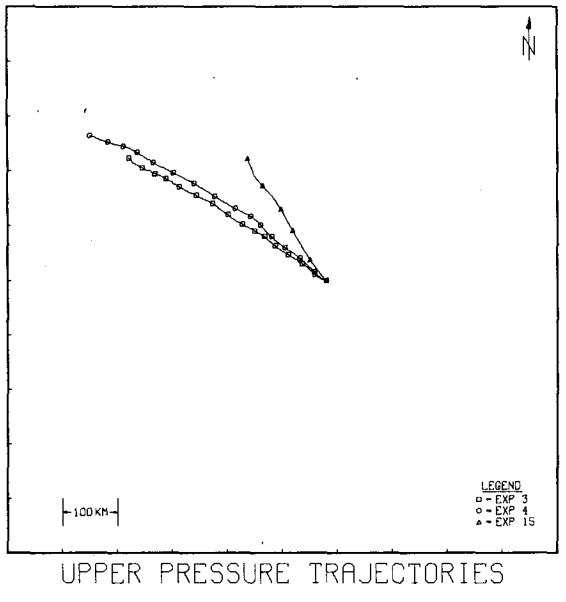

FIG. 14. Trajectories of the point of maximum upper ocean pressure for EXP 3 (20/4) for 150 days, EXP 4 (30/6) for 150 days and EXP 15 (100/20) for 50 days. Data points are placed along the paths every 10 days, and the starting position of EXP 15 has been moved 100 km to the North for purposes of comparison (see Appendix B).

when one considers that the barotropic and baroclinic pressures may not yet have evolved to their appropriate modon values, as the direction of travel is slightly northward.

4. Experimental results

a. Trajectories and propagation velocities

In Section 3, it was noted that the tendency of all eddies of types A, B and C (in the absence of a mean current) is to propagate toward the west, while the rate of northward propagation of cyclonic rings is determined by their current strength. In this section, we quantify these arguments by presenting northward and westward propagation speeds, and showing the dependence of some of these on nonlinearity ($U_1/\beta l^2$) and the barotropic ratio ($\max U_2/\max U_1$).

As $U_1/\beta l^2$ is increased for constant barotropic ratio, planetary vorticity is advected from north and south of the eddy to either side at a greater rate than would be the case for a smaller nonlinearity. This results in a faster translation to the west and to the north. These tendencies may be seen in Fig. 14, which contains the trajectories of the point of

minimum upper ocean pressure ($\min P_1$) for EXP 3 (a 20/4 ring), EXP 4 (30/6) and EXP 15 (100/20). These vortices are upper ocean eddies with $\max U_2/\max U_1 = 0.2$, and the behavior of the northward and westward propagation rates with increasing nonlinearity is evident. Data points are placed every 10 days and we can clearly see that both northward and westward propagation velocities increase with increasing $U_1/\beta l^2$. Moreover, as the eddy weakens, its rate of northward progress lessens, and propagation is directed more toward the west; this tendency is very noticeable in EXP 3 and EXP 4.

Although the tendency for an eddy to propagate more rapidly westward as $U_1/\beta l^2$ is increased is also evident for $\max U_2/\max U_1 = 0.0$ (Fig. 15), the results for barotropic propagation ($\max U_2/\max U_1 = 1.0$) do not exhibit this trend. We conjecture that the reason for this may be found by examining the pressure contours for EXP 5 (Fig. 5) which indicate that so much of the eddy energy has been lost by day 50 that the trailing anticyclonic vortex has a larger absolute value of the central pressure and may in fact significantly alter the propagation velocity of the cyclonic eddy. Thus, these barotropic propagation velocities may be vitiated by motions external to the eddy of principal interest.

Although the Firing and Beardsley (1976) eddies have zonal propagation velocities which are too small (1.06 km day^{-1}—see Appendix A) to appear on Fig. 15, we are encouraged by the fact that the westward speed of the Bretherton and Karweit (1975) upper ocean ring is very consistent with the present data. The barotropic ratio is 0.03 and corresponds to a speed which lies very slightly below the curve of $\max U_2/\max U_1 = 0.2$. This data point and most of the other results thus appear consistent

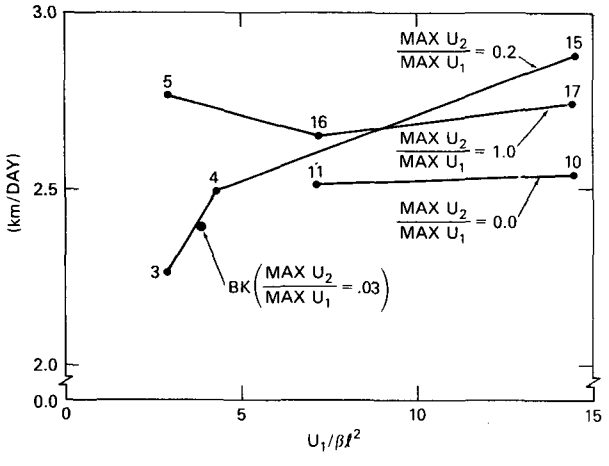

FIG. 15. The westward propagation velocities as a function of nonlinearity ($U_1/\beta l^2$) for constant barotropic ratios ($\max U_2/\max U_1 = 0.0$, 0.2, and 1.0). The numbers beside each data point refer to a 26-day speed average for that experiment, and BK denotes the Bretherton and Karweit (1975) ring (see Appendix A).

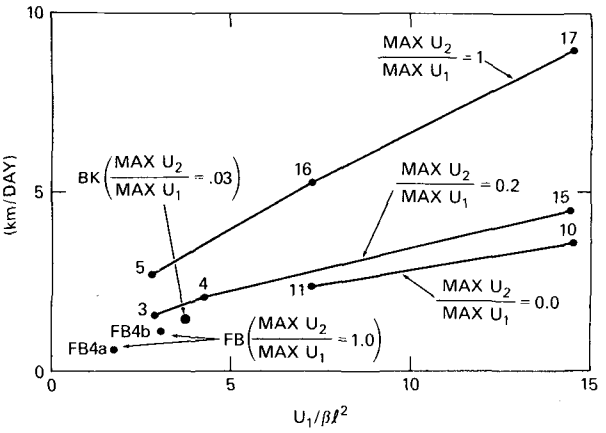

FIG. 16. The northward propagation velocities as a function of nonlinearity ($U_1/\beta l^2$) for constant barotropic ratios ($\max U_2/\max U_1 = 0.0$, 0.2, and 1.0). The experiment number is given beside each data point and represents a 26-day average of the speed data; BK is the Bretherton and Karweit (1975) eddy and FB4a and FB4b are Firing and Beardsley's (1976) Figs. 4a and 4b (see Appendix A).

with the expected trend that as the barotropic ratio is increased for a constant $U_1/\beta l^2$, the propagation velocity increases.

In the same vein, the northward propagation rates become greater with increasing $U_1/\beta l^2$ for constant $\max U_2/\max U_1$ (see Fig. 16). As the barotropic ratio is increased, while $U_1/\beta l^2$ is held fixed, the meridional velocity can be seen to increase; and none of the anomalous behavior noted in the zonal propagation rates for barotropic rings is evident in these northward propagation speeds. Moreover, both the Bretherton and Karweit eddy and the Firing and Beardsley vortices appear to have a northward velocity very consistent with the data of the present work.

For strongly nonlinear eddies ($U_1/\beta l^2 = 14.41$) we have performed experiments on rings in which the barotropic ratio is increased from 0.0 (EXP 10—a 100/0 eddy) to 1.2 (EXP 13—a 100/120 eddy) and the northward propagation speed is a strong function of $\max U_2/\max U_1$, (Fig. 17). We would expect the meridional velocity to increase as the barotropic ratio becomes larger because, generally speaking, the entire water column is more vigorously advecting planetary vorticity from the north and south around the periphery of the eddy, and the increase in propagation rate is expected.

b. Evolution of the pressure extremum

Unless acted upon by external influences, the minimum pressure within the core of a cyclonic ring can be altered by either a decay of the energy of the flow by subgrid-scale processes or through the efflux of eddy energy by radiating waves. These two phenomena can in turn be altered by changing the strength of the nonlinearity, the barotropic ratio and

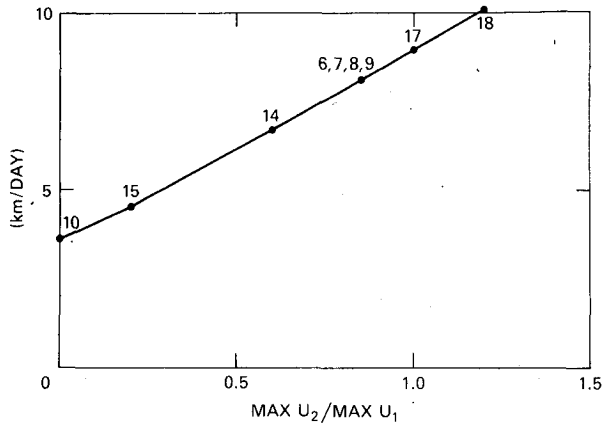

FIG. 17. The northward propagation velocities as a function of $\max U_2/\max U_1$ for $U_1/\beta l^2 = 14.41$. The numbers beside the data points indicate the experiment number. The speeds are obtained by taking an average of the first 26 days' data.

the kinematic viscosity. In this subsection, we examine the behavior of the pressure extremum as it is influenced by the parameters $U_1/\beta l^2$, $\max U_2/\max U_1$ and A_H.

When an initially circular ring is placed in the box at the start of the experiment, evolution toward a preferred configuration begins immediately because only the crude assumption of geostrophy on an f-plane has been made. This rapid correctional readjustment, together with the expected subsequent evolution of the eddy, radiates barotropic and baroclinic Rossby waves, as well as some internal wave energy. When the most rapidly traveling of these waves reach the walls of the box, they are reflected and may propagate into their region of generation in the vicinity of the eddy, contaminating the time record of the pressure in the center of the ring. The effects of this process have been examined in somewhat greater detail (Appendix B) and we have concluded that the experiments may be considered unaltered by what we term wall effect for the first 25 days or so.

Because the deep and upper ocean pressures are related through $\nabla P_2 = \nabla P_1 + g'\nabla h$, and the influence of the reduced gravity is relatively small, the deep ocean pressure extremum as a function of time bears a qualitatively similar appearance to that for the upper ocean in general. Moreover, in the case of upper ocean eddies, the only meaningful pressure in either of the two layers is that in the upper ocean; for these reasons, we will almost always discuss a ring in terms of P_1, nondimensionalized by its value at $t = 0$. Focusing on only P_1 represents a unifying thread of another sort. For eddies which are barotropic—or nearly so—and those which are upper ocean rings from the start, the behaviors of the $P_1(t)$ time records are quite similar. In Fig. 18a, the results of EXP 14 are shown for 50 days. Although wall influence becomes important after 25 days, the record possesses two features whose presence is only slightly modified by this effect. Specifically, there is a general decline of the minimum $P_1(t)$, and there exists a plateau and slight increase in P_1 between days 20 and 35. The decay of the pressure can be attributed partly to the strength of the nonlinearity and partly to the influence of viscosity. We shall investigate the relative influences of A_H, $\max U_2/\max U_2$ and $U_1/\beta l^2$ below, but the odd behavior of the pressure between days 20 and 35 merits our attention first. In Figs. 18b and 18c, we see a record of P_{BT} and P_{BC} also for the first 50 days, and we note that this feature is present only in the barotropic pressure. The effect which raises the pressure in the center of the eddy is thus present throughout the water column and exists in all experiments at about the same time, for the same time interval, but to varying degrees. In Figs. 18d and 18e, we see the contours of constant barotropic and baroclinic pressure at 25 days; and, we note that the trailing anticyclonic vortex behind the main cyclonic feature is a largely barotropic phenomenon. We thus attribute this temporary P_{BT} increase to the presence of the southwestward propagation of the elongated trailing anticyclonic motion, the closest approach of which to the main cyclonic eddy occurs during the time interval 20–35 days. Bearing this in mind, we will now briefly discuss the effects of changes in the nonlinearity, barotropic ratio and eddy viscosity on the propagation.

1) THE ROLE OF NONLINEARITY

The effect of very weak ring currents is to allow the initially circular eddy to rapidly disperse (EXP 13, Fig. 4), so that we might intuitively expect that an increase in the nonlinearity $U_1/\beta l^2$ would result in a less rapid decrease in the eddy pressure for constant barotropic ratio $\max U_2/\max U_1$. This is because the eddy would be expected to propagate relatively unchanged, radiating less of its energy away as waves. This is, in fact, observed to be the case. In Fig. 19a $P_1(t)$ is shown for EXPs 3, 4 and 15 ($\max U_2/\max U_1 = 0.2$); and, Fig. 19b gives $P_1(t)$ for EXPs 10 and 11 ($\max U_2/\max U_1 = 0.0$). In each figure, a family of curves appears in which only $U_1/\beta l^2$ is changed. Although the central pressure in the most nonlinear rings can change immediately after initialization for reasons discussed above, we can clearly see that the pressure decay of the stronger rings after the period of initial readjustment is more gradual; thus, an increase in the strength of the current results in a vortex which is longer lived than the weaker ones. In particular, the most nonlinear of the three in Fig. 19a (EXP 15) has the largest central pressure at day 25, while Fig. 19b indicates that despite a fairly rapid initial decline in the pressure in EXP 10, this more strongly nonlinear case experiences such a gradual pressure decay, that the

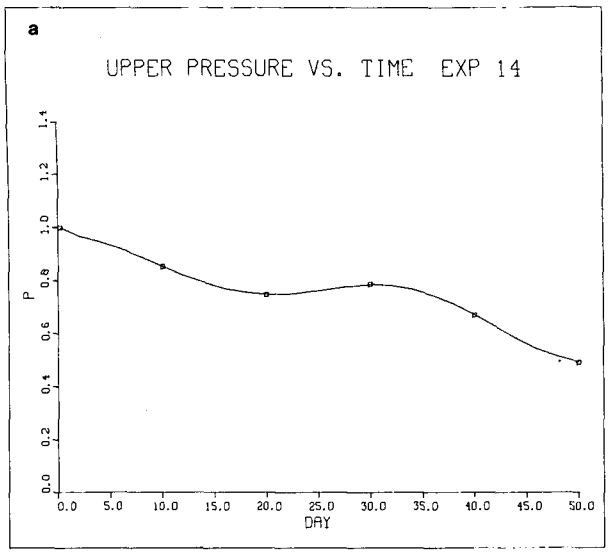

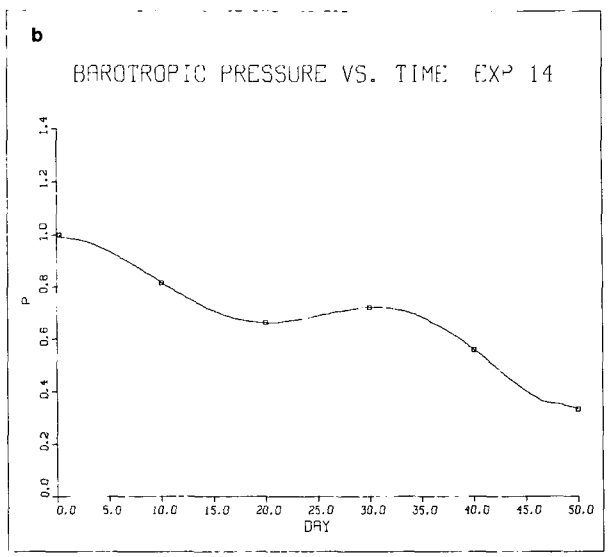

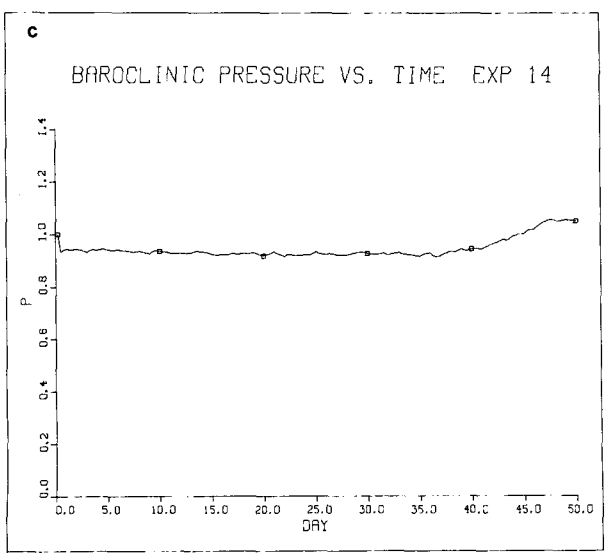

FIG. 18a–c. Fifty-day records of the central pressure extremum for EXP 14, nondimensionalized by their value at $t = 0$ (a). Upper ocean pressure $P_1(t)$. (b) Barotropic pressure $P_{BT}(t)$. (c) Baroclinic pressure $P_{BC}(t)$. The small-scale fluctuations are presumed to be due to the presence of internal waves.

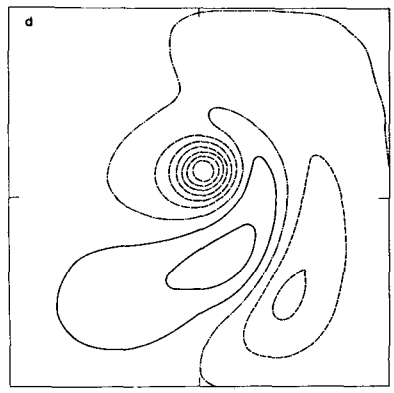

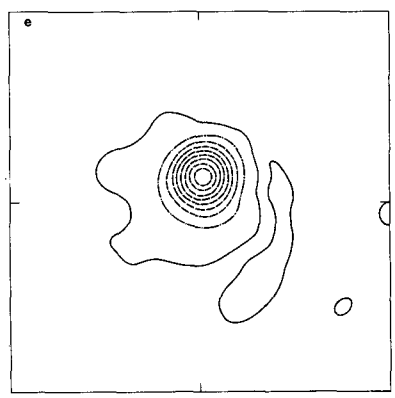

FIG. 18d–e. Contours of constant pressure at day 25 for EXP 14. Contour code: (-----) for $P < 0$; (– – –) for $P = 0$; and (——) for $P > 0$. (d) Barotropic pressure P_{BT}. Contour level = 0.5 $m^2 s^{-2}$. (e) Baroclinic pressure P_{BC}. Contour level = 0.14 $m^2 s^{-2}$. The only positive P_{BC} contour level = 0.07 $m^2 s^{-2}$.

weaker, more rapidly decaying EXP 11 pressure has declined to the point where they are both equal by day 25. From Figs. 19a and 19b, however, we can see that the pressure is not a strong function of the nonlinearity, whenever $U_1/\beta l^2$ is large.

2) THE EFFECT OF THE RELATIVE STRENGTH OF THE BAROTROPIC FLOW

A relatively large number of the experiments performed (Fig. 2) are for constant nonlinearity ($U_1/\beta l^2 = 14.41$) and different initial barotropic ratios ($\max U_2/\max U_1$). This change in the value of $\max U_2$ for fixed $\max U_1$ allows us to effectively alter the relative strength of the barotropic component of the flow. For EXPs 10, 15, 14, 7 and 17, the values of $\max U_2/\max U_1$ are 0.0, 0.2, 0.6, 0.85 and 1.0, respectively. As the value of the barotropic ratio is increased from zero to unity, the barotropic com-

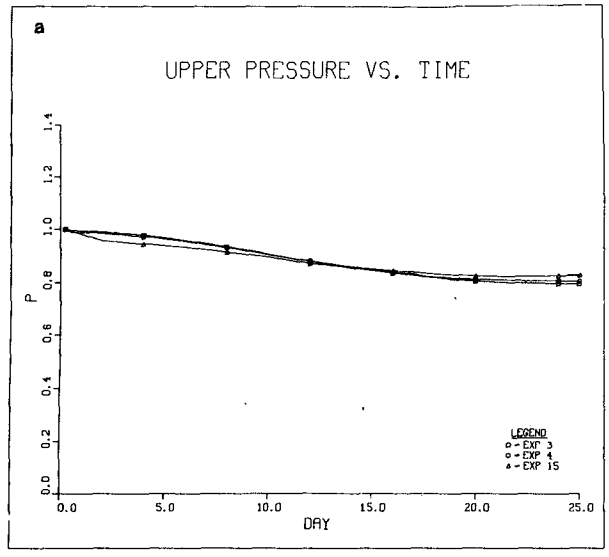

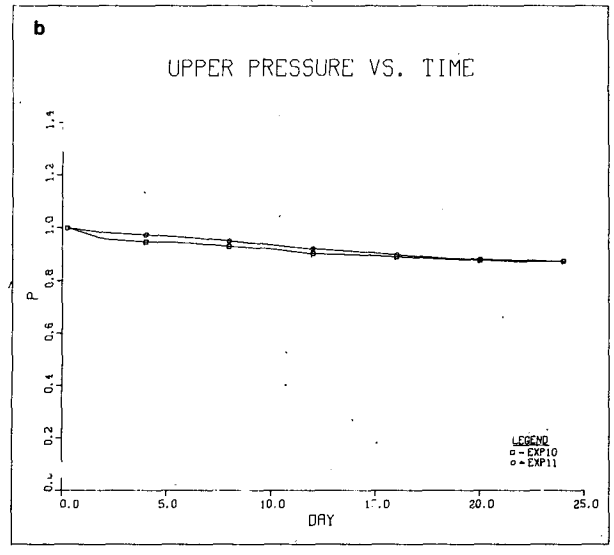

FIG. 19. Effect of changing $U_1/\beta l^2$ on nondimensionalized minimum pressure $P_1(t)$ in upper ocean. (a) $P_1(t)$ for EXP 3, 4, 15 with $\max U_2/\max U_1 = 0.2$. (b) $P_1(t)$ for EXP 11 and 10 with $\max U_2/\max U_1 = 0.0$.

ponent of the current is a concomitantly larger portion of the initial flow in the ring. Because these rings are weakly dispersive, and barotropic waves propagate so much more rapidly than the baroclinic ones, we can see (Fig. 20) that a systematic increase in $\max U_2/\max U_1$ results in a progressively more rapid decrease of the upper ocean pressure.

3) THE INFLUENCE OF VISCOSITY

It is interesting to assess the effect of changing the lateral viscosity A_H because we are ever aware of the elementary fashion in which it parameterizes the energy dissipation by subgrid-scale processes. In Fig. 21, the results of EXP 14 ($A_H = 2.5 \times 10^5$ cm^2 s^{-1}), EXP 19 ($A_H = 5 \times 10^5$ cm^2 s^{-1}) and EXP 20 ($A_H = 2.5 \times 10^6$ cm^2 s^{-1}) are presented. By day 25, the nondimensionalized minimum pressure in EXP 20 lies well below that of EXP 19, which in turn lies below that of EXP 14. These is thus a strong dependence of the upper ocean pressure upon viscosity. This is really somewhat surprising because we would intuitively expect nonlinearity to be more important in maintaining the central pressure. EXP 20 represents a factor of 10 increase in A_H over that of EXP 14, while EXP 15 represents a factor of 5 increase in $U_1/\beta l^2$ over that of EXP 3. In the first case there is a significant difference in the rate of P_2 decay; in the second, hardly any.

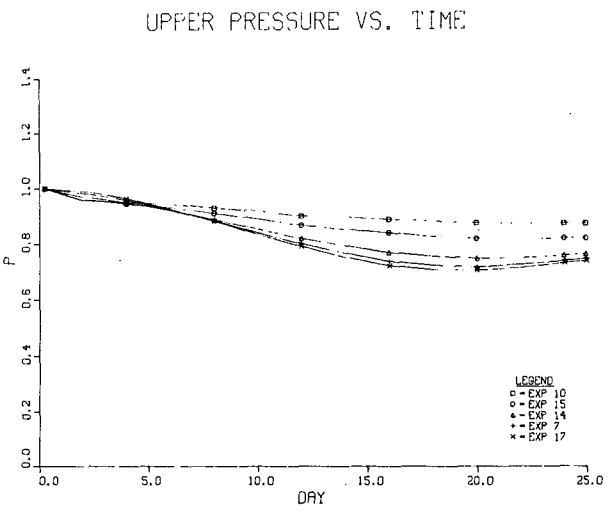

FIG. 20. Upper ocean pressure $P_1(t)$ for increasing $\max U_2/\max U_1$: EXP 10 (100/0), EXP 15 (100/20), EXP 14 (100/60), EXP 7 (100/85), and EXP 17 (100/100). $U_1/\beta l^2 = 14.41$ in all cases.

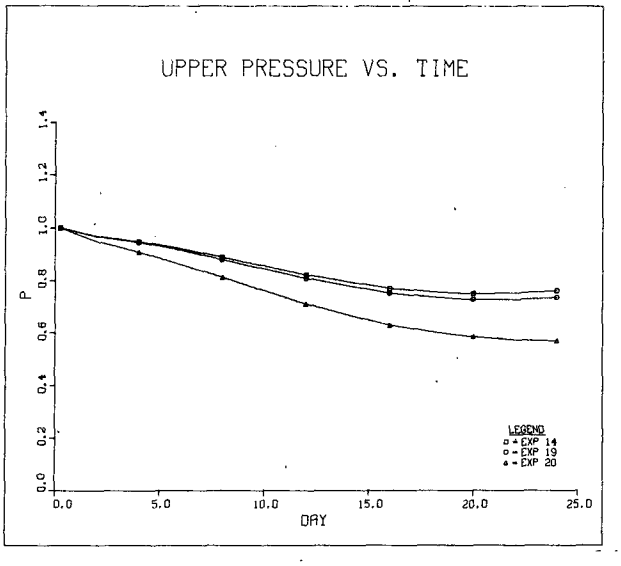

FIG. 21. Effect of increasing eddy viscosity upon ocean pressure. EXP 14, $A_H = 2.5 \cdot 10^5$ cm^2 s^{-1}; EXP 19, $A_H = 5 \cdot 10^5$ cm^2 s^{-1}; EXP 20, $A_H = 2.5 \cdot 10^6$ cm^2 s^{-1}.

These results indicate that the rate of energy loss in the ring can be extremely sensitive to the value of the eddy viscosity used, but fairly insensitive to the magnitude of the nonlinearity present, as long as $U_1/\beta l^2$ is sufficiently large to maintain the eddy against rapid linear dispersion. A consequence of this observation is also that considerable attention should be paid to the manner in which subgrid-scale processes are treated in ring propagation studies.

c. *Departure from geostrophy*

One of the largest benefits in using a primitive equation model is that no *a priori* order-of-magnitude assumptions are made regarding Coriolis and pressure gradient forces, as in the case of a quasi-geostrophic formulation. While we do not know which portions of the velocity and pressure field are geostrophic and ageostrophic, we can nevertheless obtain an excellent overall qualitative impression of the extent to which the direction of the current is related to the gradient of the pressure fields in the upper and deep oceans. In Figs. 22a and 22b the contours of constant P_1 and P_2 for EXP 7 at day 25 are shown, over which are superimposed arrows indicating velocity fields. The center of the arrow gives the position of the particle whose speed is designated by that arrow. Except for the very limited portion of the flow which is between the main eddy and the trailing anticyclonic high, Fig. 22 indicates that tangents to the lines of constant pressure are remarkably close to being parallel to the local current direction. We thus suspect that the assumption of quasi-geostrophy for this type of flow may be quite good. A definitive answer, however, must await the outcome of a more quantitative intercomparison between current magnitudes calculated by both the primitive equation and the quasi-geostrophic models.

5. Conclusion

This paper has sought to examine some aspects of the propagation and evolution of cold-core Gulf Stream rings through the use of a two-layer primitive equation beta-plane model in a 1000 km square box. The central pressure of the evolving eddy is shown to be independent of the influence of the wall for the first 25 days of the experiments. Eighteen of these experiments have been performed for simulated time intervals of 50 and 150 days, and information has been obtained on the zonal and meridional propagation rates, and the behavior of the central eddy pressure for differing horizontal viscosities (A_H), nonlinearities ($U_1/\beta l^2$) and barotropic ratios ($\max U_2/\max U_1$).

The rings presented in this work are found to belong to four classes: dispersing, barotropic and nearly barotropic, upper ocean and eastward-propagating eddies. Dispersing vortices possess

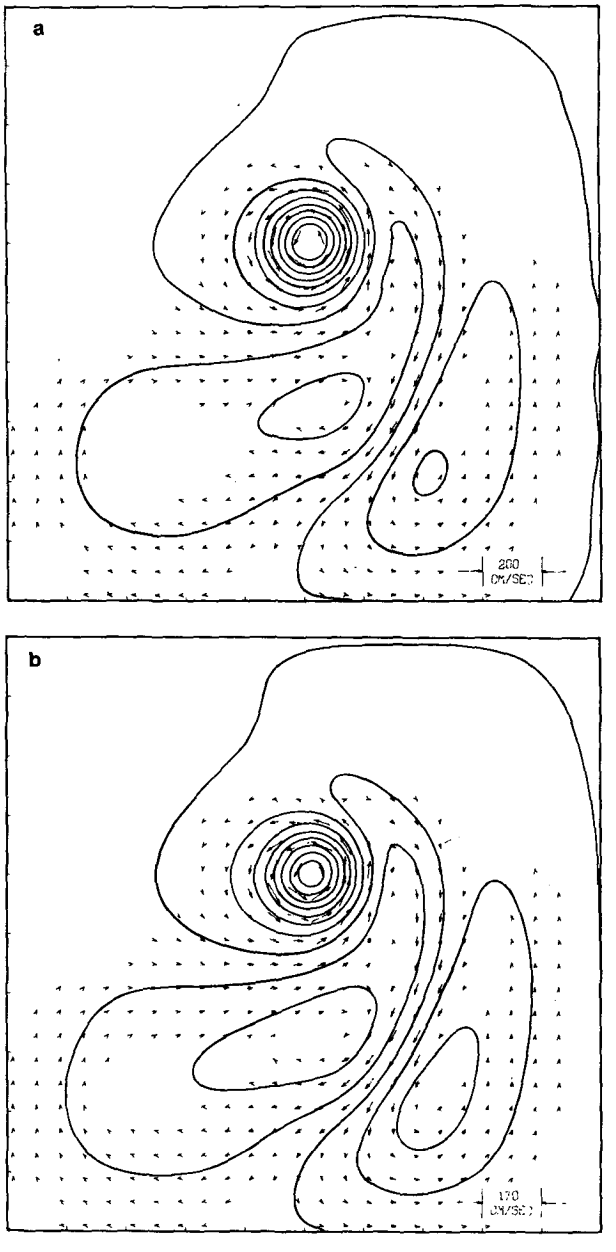

FIG. 22. Lines of constant pressure for EXP 7 at day 25 superimposed on the velocity field; arrows are deleted whenever $u_i^2 + v_i^2 \leq 10$ cm^2 s^{-2}. (a) The upper ocean, contour level = 0.7 m^2 s^{-2}; (b) the deep ocean, Contour level = 0.6 m^2 s^{-2}.

insufficient nonlinearity to propagate intact; EXP 13 is such a structure and the baroclinic pressure as a function of time agrees well with the linear quasi-geostrophic (Fig. 4) result of Flierl (1977).

If the velocities in the upper and deep ocean are different initially, one might expect that the mechanism of vortex stretching would eventually effect a state of barotropy. For small H_1/H_2, however, the effect of the vortex stretching is insufficient to effectively couple the bottom fluid to the upper ocean. A ripid barotropic-like dispersion of the deep-

ocean gyre ensues and—in the case of nearly barotropic eddies—the central pressure P_2 is observed to decay much more rapidly than P_1. The upper ocean eddies, on the other hand, possess insufficient deep-ocean nonlinearity to maintain the lower gyre for any length of time at all; and there is never any real vortex present in the deep ocean.

Although the experiments were necessarily valid for only a fairly short duration, we conjecture that the relatively rapid decay of P_2 (vis-a-vis P_1) for nearly barotropic rings indicates that these vortices ultimately evolve to upper ocean eddies. The results of this paper would thus seem to indicate that the upper-ocean eddy may be a state to which Gulf Stream rings in a shallow thermocline ocean ($H_1/H_2 \ll 1$) with no external shear might evolve, given sufficient time.

An elementary extension of the work of Flierl *et al.* (1980) to restrict the vorticity to be continuous everywhere appears to yield results for propagation speed and modon radius which are in tolerably good agreement with the results of EXP 12. The small deviation from eastward propagation is tentatively ascribed to the fact that the cyclonic barotropic vortex is somewhat more intense than the associated anticyclonic one and is assumed to result in the observed slow drift to the north.

Upper ocean eddies and barotropic (or nearly barotropic) eddies possess a westward phase speed which increases with increasing nonlinearity and increasing barotropic ratio (Fig. 15) and possess a northward phase speed which also increases with increasing nonlinearity (Fig. 16) for constant barotropic ratio. For large nonlinearity, the northward propagation rate increases with increasing barotropic ratio (Fig. 17).

For fixed barotropic ratio an increase in the nonlinearity of upper ocean eddies and nearly barotropic rings results in a somewhat slower rate of decay of the central pressure (Figs. 19a and 19b). The longevity of the eddy, however, does not appear to be a strong function of $U_1/\beta l^2$ provided the value of the nonlinearity is sufficiently large to prevent rapid linear dispersion of the ring by its constituent Rossby waves. In contrast to this, the central pressure in the upper ocean is very sensitive to the value of the eddy viscosity used (Fig. 21), with the upper ocean pressure rolling off noticeably more sharply when A_H is increased by a factor comparable to the above increase in nonlinearity. We thus infer that an intensely nonlinear ring in a hypothetical nondissipative ocean would persist for a very long time.

And finally, one must ask the question of whether the expense of a primitive equation model is justified over that incurred when the calculations are performed with a quasi-geostrophic model. Figs. 22a and 22b indicate that there exist only small regions of the flow in which the velocity is not tangent to the pressure gradient. This argument, however, does not address the matter of current magnitudes. Whether a discrepancy between the currents calculated with the two types of models is sufficient to alter the aggregate properties of the eddy can only be ascertained after a direct comparison between results of the same calculation performed with both models.

Acknowledgments. The authors with to thank one of the reviewers of an earlier draft (Mied, 1978a), who suggested that the work might benefit from a larger number of experiments and a wider range of parameters. In addition, we wish to thank Prof. G. R. Flierl for providing us with a first draft of the paper by Flierl *et al.* (1980), for sending us his tabulations of our modon dispersion equations in our Section 3d, and for discussions which led to our modon spinup simulation in EXP 12. We wish also to thank Dr. J. C. McWilliams for an interesting discussion on the merits of using the orthonormal baroclinic and barotropic pressures and for sending us a copy of the manuscript by McWilliams and Flierl (1979). The authors are also grateful to Dr. L. B. Lin for answering several questions about the Holland and Lin (1975) code, and to Dr. J. D. Thompson for some general guidance on numerical computations.

APPENDIX A

Connection with Other Work

1. The quasi-geostrophic model

In the absence of damping, the quasi-geostrophic equations for a two-layer medium are written (Pedlosky, 1964; Rhines, 1976) as

$$\frac{D}{Dt}\left[\nabla^2\psi_1 + F_1(\psi_2 - \psi_1)\right] + \beta\frac{\partial}{\partial x}\psi_1 = 0,$$

$$\frac{D}{Dt}\left[\nabla^2\psi_2 + F_2(\psi_1 - \psi_2)\right] + \beta\frac{\partial}{\partial x}\psi_2 = 0,$$

where $F_i = f_0^2/(g'H_i)$ and $D(\ )/DT = \partial(\ )/\partial t + \partial[\psi_i,(\ )]/\partial(x,y)$. Neglecting the nonlinear terms, employing the coordinate system

$$\xi = x - ct,$$

$$\eta = y,$$

$$\tau = t,$$

and requiring steady motion in this moving reference frame, we see that

$$\nabla^2\psi_1 + F_1(\psi_2 - \psi_1) + \frac{\beta}{c}\frac{\partial}{\partial\xi}\psi_1 = 0,$$

$$\nabla^2\psi_2 + F_2(\psi_1 - \psi_2) + \frac{\beta}{c}\frac{\partial}{\partial\xi}\psi_2 = 0,$$

where $\nabla^2 = \partial^2/\partial\xi^2 + \partial^2/\partial\eta^2$. If we require that, regardless of geometry, the flows in the upper and the lower oceans be linearly dependent (have a modal structure), we may write $\psi_2 = a\psi_1$ so that the system becomes

$$\nabla^2\psi_1 + [F_1/a - (F_1 + \beta/c)]\psi_2 = 0,$$
$$\nabla^2\psi_2 + [aF_2 - (F_2 + \beta/c)]\psi_2 = 0.$$

Equating the coefficients of the linear terms, we see that

$$a = 1, -F_1/F_2,$$

which is simply the modal structure of the barotropic and baroclinic motions. As one equation will now suffice to describe the motion, we choose the latter and write for the baroclinic flow

$$\kappa^2 = -(F_2 + \beta/c) - F_1$$

or

$$c = \frac{-\beta}{\kappa^2 + Rd^{-2}},$$

where $R_d = (F_1 + F_2)^{-1/2}$ is the deformation radius. Consider now a polar coordinate system (r,θ). The analysis now proceeds identically to that of Flierl (1977). An initially circularly-symmetric disturbance is given by

$$\psi = \int_0^\infty \hat{\kappa} d\hat{\kappa} g(\hat{\kappa}) J_0(\hat{\kappa}\hat{r}),$$

where the nondimensional variables (ˆ) are

$$(x,y) = l(\hat{x},\hat{y}), \quad c = \hat{c}\beta l^2,$$
$$(u,v) = U(\hat{u},\hat{v}), \quad t = \hat{t}/(\beta l),$$
$$\psi_i = Ul\hat{\psi}_i, \quad k = \hat{\kappa}/l.$$

In dimensional variables, the pressure extremum of a pure baroclinic Gaussian eddy (with Hankel transform $g(\hat{\kappa}) = e^{-\hat{\kappa}^2/2}$) moves westward at a rate

$$V_0 = \beta l^2\{+\tfrac{1}{2} - (l^2/4R_d^2)e^{l^2/2Rd^2}E_1(l^2/2Rd^2)\},$$

where

$$E_1(z) = \int_z^\infty e^{-y}/y dy.$$

The pressure decay, nondimensionalized by the value at $t = 0$ is given as $P = 1 - (t/T)^2$, where

$$T = \frac{1}{\beta}\left[\frac{4/R_d^2}{B_1 + B_1B_2 - 2B_2}\right]^{1/2},$$
$$B_1 = xe^xE_1(x),$$
$$B_2 = x(1 - B_1),$$
$$x = l^2/2R_d^2.$$

When dealing with mixed-mode eddies, it is convenient to separate the baroclinic and barotropic components of the pressure. Since a purely baroclinic flow is one in which the *ratio* of the pressures is $+F_1/F_2 = H_2/H_1$, we add the constraint that the two vertical modes, (ϕ_α, α = barotropic, baroclinic, say) be orthonormal (Flierl, 1978), i.e.,

$$\frac{1}{H}\int_0^H \phi_\alpha\phi_\beta dz = \delta_{\alpha\beta}, \quad H = H_1 + H_2.$$

This restriction then uniquely defines the coefficient of the barotropic pressure[5] (ψ_{BT}) to be 1 in each layer and those for the baroclinic flow pressures (ψ_{BC}) to be $(H_2/H_1)^{1/2}$ in the upper ocean and $-(H_1/H_2)^{1/2}$ in the deep ocean. We may then uniquely write the upper and deep ocean pressures at a point as

$$\psi_1 = \psi_{BT} + R\psi_{BC},$$
$$\psi_2 = \psi_{BT} - \frac{1}{R}\psi_{BC}, \quad R = (H_2/H_1)^{1/2}.$$

This decomposition is suggested by the quasi-geostrophic model, but we will find it useful in our primitive equation calculations as well. It also provides a basis for rational comparison between the two models. In the present work, $H_2 = 4000$ m, $H_1 = 1000$ m so that $R = 2$ always.

2. Barotropic eddy propagation

Firing and Beardsley (1976) have studied the propagation and evolution of two cyclonic, barotropic eddies on a beta plane through the use of a linear calculation, a laboratory experiment and a nonlinear numerical model; the flows in the laboratory and numerical models show excellent agreement. The parameters of their experiment are

h_0 mean tank depth (8.0 cm)
ϵ nondimensional eddy-generating piston motion (0.084, 0.15) [$=\Delta h/ho$]
α lid slope (related to laboratory β) = 0.1
r_1 radius of eddy-generating inner piston (1.98 cm) [$=l$ in present work]
$\Omega = f_0/2 = 2\pi$ s^{-1}.

The eddy is generated by the coordinated impulsive motion of a downward-moving piston and an upward moving concentric cylinder. The initial nondimensional azimuthal velocity is given in terms of the nondimensional radius by

$$v_0 = \begin{cases} r/2, & 0 \leq r < 1 \\ -r/2 + 1/r, & 1 \leq r < 2^{1/2} \\ 0, & 2^{1/2} \leq r, \end{cases}$$

where the velocity and length scales are $2\epsilon\Omega r_1$ and r_1, respectively. The maximum dimensional velocity

[5] When discussing quasi-geostrophic dynamics, we shall use pressure and stream function interchangably. For the primitive equation experiments in this paper, the pressure is decomposed into barotropic and baroclinic constituents as is shown.

TABLE A1. The maximum currents in each layer, counting from the top of the ocean to the bottom.

Layer no.	A_r	Maximum current (cm s^{-1})	Layer thickness (km)
1	1.0	23.2	0.175
2	0.9	20.8	0.475
3	0.5	11.6	0.4
4	0.1	2.3	1.0
5	0	0	1.6
6	0	0	1.35

thus occurs at dimensional radius r_1 and equals $\epsilon\Omega r_1$. A measure of the nonlinearity in our work is $U_1/\beta l^2$, which is equivalent to $\epsilon\Omega r_1/\beta r_1^2$ in their laboratory experiment. But $\alpha f_0/h_0 = \beta$, so that

$$\frac{\epsilon\Omega}{\beta r_1} = \begin{cases} 1.70 \text{ (their Fig. 4a)} \\ 3.03 \text{ (their Fig. 4b).} \end{cases}$$

We note that their measure of the nonlinearity is a Rossby number Ro $= \epsilon h_0/\alpha r_1$, which is twice that used in the present study.

The experimental distances $(\Delta x, \Delta y)$ through which the two cyclonic eddies move[6] are $(-1.2$ cm, 0.6 cm) for Fig. 4a and $(-1.2$ cm, 1.2 cm) for Fig. 4b which, when scaled by the ratio of length scales (l/r_1) implies displacements $(-35.7$ km, $+17.9$ km) and $(-35.7$ km, $+35.7$ km) respectively, in the present work. The elapsed time in their experiments[7] is $3.42 \times h_0/(2\omega\alpha r_1) = 3.42/(\beta r_1)$, which is $3.42/(\beta l) = 33.6$ days in the present work. Propagation velocities for their two experiments are thus 1.06 km day^{-1} west, 0.53 km day^{-1} north for Fig. 4a and 1.06 km day^{-1} west, 1.06 km day^{-1} north for Fig. 4b.

3. Mixed (pure barotropic + pure baroclinic) eddies

Bretherton and Karweit (1975) have modeled the evolution and propagation of a cyclonic eddy using a six-layer quasigeostrophic model. In each layer the initial streamfunction is given by

$$\psi = -A_r U l \exp(-r^2/2l^2), \quad r = 1, 2, \ldots 6,$$

so that the azimuthal velocity $(\partial\psi/\partial r)$ has a maximum value of $+A_r U \exp(-1/2)$ located at $r = l$. Because there is disagreement between the calculated value of the maximum layer currents and their stated numerical values, there is uncertainty about the actual maximum velocities used.[8] We will assume that the above streamfunctions (hence our calculated currents) are correct, as is their value given for U. Their parameters are

$U = 33$ km day^{-1},

$l = 45$ km,

$\beta = 2 \times 10^{-3}$ km^{-1} day^{-1} $= 2.31 \times 10^{-13}$ cm^{-1} s^{-1},

and the maximum current speeds are shown for each layer in Table A1.

We may compare results from this six-layer model to our two-layer simulation by grouping together layers 1–3 (equivalent $H_1 = 1.05$ km) and layers 4–6 (equivalent $H_2 = 3.95$ km). A depth-averaged current can then be derived for the upper ocean (17.7 cm s^{-1}) and for the deep ocean (0.58 cm s^{-1}). Calculated values appropriate to the present work, subject to the ambiguity noted above, are thus (max $\times U_2$)/(max U_1) $= 0.03$, $U_1/\beta l^2 = 3.77$, $H_2/H_1 = 3.76$. The stated average propagation velocities for the 200-day experiment are 2.4 km day^{-1} westward and 1.5 km day^{-1} northward.

APPENDIX B

Validity of Experimental Results

The accuracy of the calculations in this paper is a matter of potential concern, and we have gone to some length to ensure that the experimental results do not have unacceptable errors. The basin-integrated mass (represented by the sum of ~2500 grid points) never changes by more than ±0.01–0.02%, even for the longest experiments of 150 days duration. This indicates, of course that the program is stable, for in the linear approximation

$$\frac{\partial h_i}{\partial t} = -H_i \nabla \cdot \mathbf{u}_i, \quad i = 1, 2.$$

A tendency of $\mathbf{u}_i$ to become unbounded would rapidly appear as an increase in the mass of the system.

Another point of concern is the length of time for which the results may be considered valid before the influence of the basin walls is felt. This question has been approached by conducting EXPs 6, 7, 8 and 9 which are (100, 85) rings started at different parts of the box (See Fig. B1 and Table B1.) The central pressure in the upper ocean, nondimensionalized by its initial value, is shown plotted as a function of time for 50 days in Fig. B2. We see that all of the pressures are in good agreement until about day 25, at which time the results of EXP 6 begin to differ from the rest; EXPs 7, 8 and 9 are in agreement for about 40 days, while EXPs 7 and 9 are close to each other for 50 days. In view of these results, EXPs 7 and 10–20 were started at the point (580, 400), while EXPs 3–6 were begun at (580, 500). We are forced to conclude, however, that those results of quantitative significance are valid only (conservatively speaking) for a time interval of ~25 days. For example, the northward and westward propagation

[6] E. Firing, personal communication.
[7] See footnote 6.
[8] F. P. Bretherton, personal communication.

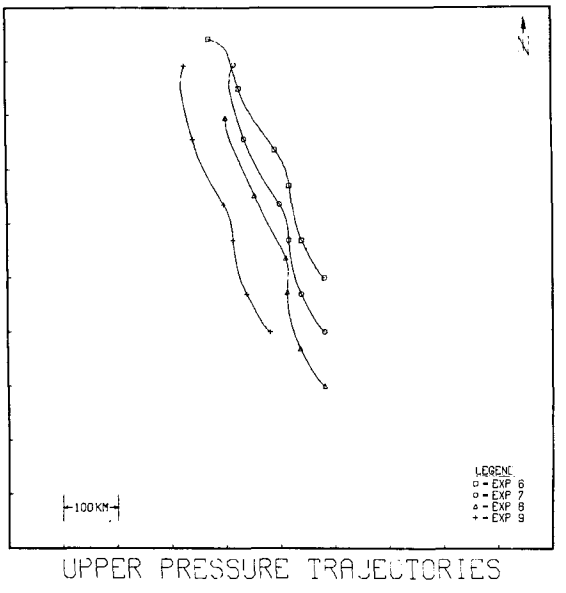

FIG. B1. The trajectories of the point of minimum upper ocean pressure P_1 for 50 days for EXPs 6, 7, 8 and 9. A data point is placed every 10 days along the paths.

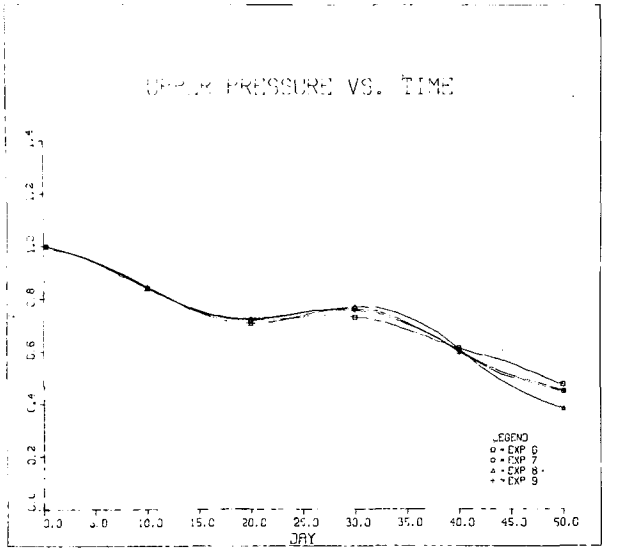

FIG. B2. The upper ocean pressures $P_1(t)$ for 50 days for EXPs 6, 7, 8 and 9.

velocities represent an average of the speeds of the eddies for the first 26 days. Whenever results at longer times are discussed, the possibility of wall influence is frequently mentioned.

A problem that arises in noting the maximum or minimum eddy pressure and its position in the box is that each of these variables is known only to the nearest grid point, which are at 20 km intervals. This is treated by searching the region in the vicinity of the eddy for the grid point at which the pressure assumes its extremum. This point then serves as the local origin for a conic section of the form,

$$P = a_{00} + a_{10}x + a_{01}y + a_{20}x^2 + a_{11}xy + a_{02}y^2,$$

which is fitted with respect to this local origin and the eight surrounding grid points by a least squares technique. The extremum in P and its location are then known. This accounts for the smooth pressure records and trajectory curves in the paper and eliminates eddy paths and pressure records having a staircase appearance which results when the location of the maximum pressure is only coarsely known to within one mesh length.

TABLE B1. The starting points [(X (km), (Y) km)] measured from the southwest corner of the box, as well as the duration of each experiment. A blank indicates no change from previous case.

Experiment	Starting point (km)	Duration (days)
3–6	(580, 500)	150
7	(580, 400)	
8	(580, 300)	50
9	(480, 400)	
10–12	(580, 400)	150
13–14		50
15		150
16–20		50

REFERENCES

Bretherton, F. P. 1975: Recent developments in dynamical oceanography. *Quart. J. Roy. Meteor. Soc.*, **101**, 705–721.

——, and M. Karweit, 1975: Mid-ocean mesoscale modeling. *Numerical Models of Ocean Circulation*, R. O. Reid, A. R. Robinson and K. Bryan, Eds., National Academy of Sciences, 237–249.

Firing, E., and R. C. Beardsley, 1976: The behavior of a barotropic eddy on a β-plane. *J. Phys. Oceanogr.*, **6**, 57–65.

Flierl, G. R., 1976: Contributions to the theory and modelling of eddies. *Theory and Modelling of Ocean Eddies: Contribution of the U. S. Delegation to the Yalta Polymode Theoretical Institute*, P. B. Rhines, Ed., 23 pp.

——, 1977: The application of linear quasi-geostrophic dynamics to Gulf Stream rings. *J. Phys. Oceanogr.*, **7**, 365–379.

——, 1978: Models of vertical structure and the calibration of two-layer models. *Dyn. Atmos. Oceans*, **2**, 341–381.

——, V. D. Larichev, J. C. McWilliams, and G. M. Reznik, 1980: The dynamics of baroclinic and barotropic solitary eddies. Submitted to *Dyn. Atmos. Oceans*.

Fuglister, F. C., 1972: Cyclonic rings formed by the Gulf Stream 1965–66. *Studies in Physical Oceanography*, A. L. Gordon, Ed., Gordon and Breach, 137–168.

Grammeltvedt, A., 1969: A survey of finite-difference schemes for the primitive equations for a barotropic fluid. *Mon. Wea. Rev.*, **97**, 384–404.

Holland, W. R., 1978: The role of mesoscale eddies in the general circulation of the ocean-numerical experiments using a wind-driven quasi-geostrophic model. *J. Phys. Oceanogr.*, **8**, 363–392.

——, and L. B. Lin, 1975: On the generation of mesoscale eddies and their contributions to the oceanic general circulation. I. A preliminary numerical experiment. *J. Phys. Oceanogr.*, **5**, 642–651.

Lai, D. Y., and P. L. Richardson, 1977: Distribution and movement of Gulf Stream rings. *J. Phys. Oceanogr.*, **7**, 670–683.

Larichev, V. D., and G. M. Reznik, 1976: Two-dimensional Rossby soliton: An exact solution. *Polymode News*, No. 19, pp. 3 and 6.

Lilly, D. K., 1965: On the computational stability of numerical solutions of time dependent non-linear geophysical fluid dynamics problems. *Mon. Wea. Rev.*, **93**, 11–26.

McWilliams, J. C., and G. R. Flierl, 1979: On the evolution of isolated nonlinear vortices. *J. Phys. Oceanogr.*, **9**, 1155–1182.

Mied, R. P. 1978a: The propagation and energetics of barotropic eddies on a beta-plane. Unpublished manuscript.

——, 1978b: Baroclinic eddy propagation and evolution on a beta plane. *Bull. Amer. Meteor. Soc.*, **59**, 889. Also presented at the *Second Conf. on Atmospheric and Oceanic Waves and Stability*, Amer. Meteor. Soc.

O'Brien, J. J., and H. E. Hurlburt, 1972: A numerical model of coastal upwelling. *J. Phys. Oceanogr.*, **2**, 14–26.

Pedlosky, J., 1964: The stability of currents in the atmosphere and the ocean: Part I. *J. Atmos. Sci.*, **21**, 201–219.

Rhines, P. B., 1976: The dynamics of unsteady currents. *The Sea*, Vol. 6. E. D. Goldberg, I. N. McCave, J. J. O'Brien and J. H. Steele, Eds., Wiley, 187–318.

Stern, M. E., 1975: Minimal properties of planetary eddies. *J. Mar. Res.*, **33**, 1–13.